''BABEŞ-BOLYAI'' UNIVERSITY
FACULTY OF PHYSICS
&
INTERDISCIPLINARY RESEARCH
INSTITUTE IN BIO-NANO-SCIENCES

**Florentina Giorgiana TALOŞ**

# *The study of nanostructured porous materials prepared by Sol-Gel method*

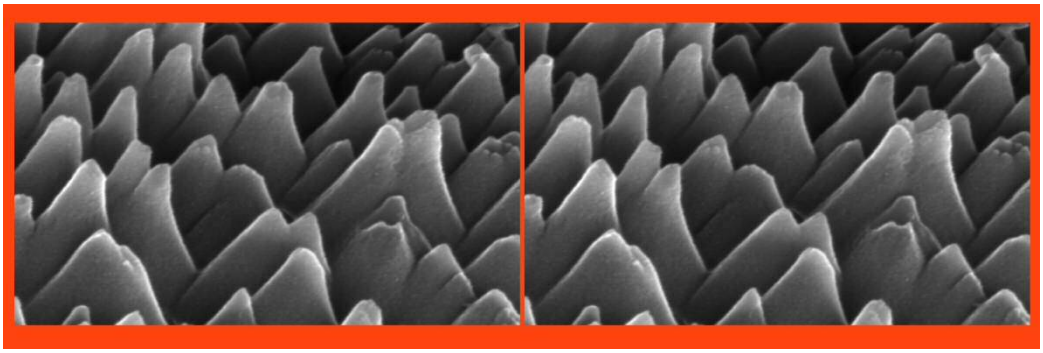

PhD Thesis Summary

*Scientific supervisor:*

**Prof. Dr. Simion SIMON**

Cluj-Napoca

***-2012-***

''BABEŞ-BOLYAI'' UNIVERSITY
FACULTY OF PHYSICS
&
INTERDISCIPLINARY RESEARCH
INSTITUTE IN BIO-NANO-SCIENCES

**Florentina Giorgiana TALOŞ**

# *The study of nanostructured porous materials prepared by Sol-Gel method*

PhD Thesis Summary

*Scientific supervisor:*

**Prof. Dr. Simion SIMON**

Cluj-Napoca

***-2012-***

# Table of Contents



***Keywords:*** sol-gel transition, rheology, Young's modulus, DTA/TGA, XRD, FTIR, BET, BJH, nanocrystals, bioactivity

# 1. INTRODUCTION

This thesis is focused on the synthesis and characterization of two classes of porous nanocomposite materials: $SiO_2$-CaO-$P_2O_5$ and $SiO_2$-CaO-$P_2O_5$-$TiO_2$, obtained by sol-gel method. Recent reports have shown the possibility of producing inorganic oxide materials by different synthesis routes including the sol-gel method [1], pulsed laser deposition [2] and plasma sprayed [3] chemical vapour deposition [4]. The sol-gel process opened new perspectives in affording materials with high purity and homogeneity, low temperature of processing and also facile incorporation of different transition metal oxides. Among the different oxides that can be embedded in the silica matrix, $TiO_2$ was selected because of its well known property of sterilization regarding the microbes [5], its good cell adhesion and proliferation [6] and also good bioactivity [7].

The main objective of this work is to monitor by rheological measurements the different kinetic mechanisms produced by chemical modifiers during the sol-gel cross-linking. The different dynamic oscillatory measurements performed with a rheometer can provide explanations for the gelation mechanism. Successively, the growing of active phase ($TiO_2$) together with the ''host'' porous silica matrix was pursued by means of drying and annealing processes. Therefore, the key points of obtaining nanostructured porous materials with specific design consist firstly in understanding the sol-gel transition and secondly in finding methods for obtaining regular structures by controlling the drying and densification processes. It was also addressed a particular attention to understand the mechanisms involved in the efficient apatite layer formation occuring on bioactive surfaces in contact with simulated body fluid (SBF).

The thesis is structured into four chapters, followed by conclusions, references, list of publications and conferences.

The **1st chapter** presents a short overview of different strategies for improving the materials bioactivity and of the general applications of silica-calcium-phosphate and $TiO_2$-nanocomposites.

The **2nd chapter** is focused on describing the differences between the physical and chemical gels, together with different mechanisms involved in the sol-gel process. In this chapter are also described the different concepts used in rheology and the various testing methods from this field.

The experimental techniques used for sample characterization will be described in the **3rd chapter** namely: rheology, compression tests, thermal analysis, X-ray diffraction, specific surface area and porosimetry, Fourier transform infrared spectroscopy, X-ray photoelectron spectroscopy, inductively coupled plasma-atomic emission spectroscopy, scanning electron microscopy and transmission electron microscopy.

The main part of this thesis is the **4th chapter** which presents the experimental results and is divided into four sections. The first section describes the synthesis of silica-calcium-phosphate materials emphasizing the motivation of the selected method and precursors, together with the different techniques used for structural and

morphological characterizations. In the second part is presented the effect of different amounts of $TiO_2$ and chelating agents embedded in the silica-calcium-phosphate matrix. The third part comprises the study of the effect of different amounts of $TiO_2$ without chelating agent added to the ternary silica-calcium-phosphate matrix. Therefore, physical and chemical analyses were performed in order to establish the optimal amount of both $TiO_2$ and $SiO_2$ that respond to the main objectives described above. The final target of this chapter is to evaluate the samples bioactivity in contact with simulated body fluid (SBF).

# 2. MATERIALS AND METHODS

## 2.1. Samples preparation

### 2.1.1 Synthesis of silica-calcium-phosphate glasses

Samples belonging to the ternary $4SiO_2$-CaO-$0.3P_2O_5$ and $2SiO_2$-CaO-$0.3P_2O_5$ systems respectively (4Si and 2Si) (see Table 1) were prepared via sol-gel method.

**Table 1. Nominal composition (mol %) of the sol–gel glasses**

| Sample Notation | $SiO_2$ | CaO | $P_2O_5$ |
|---|---|---|---|
| **4Si** | 75.5 | 18.8 | 5.7 |
| **2Si** | 60.6 | 30.3 | 9.1 |

Tetraethyl orthosilicate TEOS, ($Si(OC_2H_5)_4$, Merck), calcium nitrate ($Ca(NO_3)_2 \cdot 4H_2O$, VWR Prolabo) and di-ammonium hydrogen phosphate ($(NH_4)_2HPO_4$, VWR Prolabo), were the used reagents for the synthesis. The selected catalyst was the nitric acid ($HNO_3$) (65%, Merck). The solvent chosen for the TEOS alkoxide was its parent alcohol, the ethanol ($C_2H_6O$, EtOH) and the polymerization reactant was deionized water. All the reagents and solvents were analytical-grade quality, purchased commercially and used without any further purification. Firstly, tetraethyl orthosilicate (TEOS, ($Si(OC_2H_5)_4$) was mixed with EtOH on a magnetic stirrer at 400 rpm for 30 minutes at a molar ratio TEOS: EtOH = 1.02: 2.04. In order to trigger the reactions of TEOS, another liquid media was added, namely $H_2O$: $HNO_3$: EtOH= 0.22: 0.17: 0.31. All the hydrolysis reactions of the reagents were performed at room temperature. The calcium and phosphorus salts were separately dissolved in deionised water for 30 minutes, according to the molar ratio 0.51: 1.02. The further addition of phosphorus into calcium solution produced a white precipitate. The nitric acid (65%) was added to this white precipitate in a ratio of 0.17. Afterwards, the solution made from TEOS/EtOH/$H_2O$/$HNO_3$ was added drop wise into the mixture of $Ca(NO_3)_2 \cdot 4H_2O$/ $(NH_4)_2HPO_4$/ $HNO_3$ under continuous stirring for 1 hour at 37°C keeping the pH at 1. Macroscopic observations had shown that the obtained samples were homogeneous and transparent.

### 2.1.2 Synthesis of silica-calcium-phosphate glasses with $TiO_2$ and chelating agent

Samples belonging to the quaternary $xTiO_2$ (100-x) [$4SiO_2$-CaO-$0.3P_2O_5$] and $xTiO_2$ (100-x) [$2SiO_2$-CaO-$0.3P_2O_5$] systems with x= 5 and 20 mol% $TiO_2$ (denoted as 4Si-5Ti, 4Si-20Ti, 2Si-5Ti, 2Si-20Ti) (Table 2) were prepared by sol-gel method.

**Table 2. Nominal composition (% mol) of the sol–gel glasses**

| Sample Notation | $SiO_2$ | CaO | $P_2O_5$ | $TiO_2$ |
|---|---|---|---|---|
| **4Si-5Ti** | 71.7 | 17.92 | 5.38 | 5 |
| **4Si-20Ti** | 60.38 | 15.10 | 4.52 | 20 |
| **2Si-5Ti** | 57.60 | 28.77 | 8.63 | 5 |
| **2Si-20Ti** | 48.48 | 24.24 | 7.28 | 20 |

Tetraethyl orthosilicate TEOS, ($Si(OC_2H_5)_4$, Merck), calcium nitrate ($Ca(NO_3)_2 \cdot 4H_2O$, VWR Prolabo) di-ammonium hydrogen phosphate ($(NH_4)_2HPO_4$, VWR Prolabo) and Titanium (IV) isopropoxide ($C_{12}H_{28}O_4Ti$, $Ti(OPr^i)_4$, 98%, Merck) were used as reagents for the synthesis. The selected catalyst was the nitric acid ($HNO_3$) (65%, Merck). The solvent chosen for TEOS and TTiP alkoxides was ethanol ($C_2H_6O$, EtOH) and the polymerization reactant was deionized water. All the reagents and solvents were analytical-grade quality, purchased commercially and used without any further purification. Firstly, tetraethyl orthosilicate (TEOS, ($Si(OC_2H_5)_4$) was mixed with EtOH on a magnetic stirrer at 400 rpm for 30 minutes. In order to trigger the reaction, another acidified media ($H_2O$/ $HNO_3$/ EtOH) was added. All the reactions of the reagents were performed at room temperature. The calcium and phosphorus salts were separately dissolved in deionized water for 30 minutes. The further addition of phosphorus into calcium solution induced a white precipitate that was dissolved with nitric acid (65%) in order to obtain a transparent sol. The chelating agent, acetylacetone, was added to the formed solution of Ti ($OPr^i$)$_4$ with ethanol in order to reduce its reactivity and were mixed together for 30 minutes. Afterwards, the solution made from TEOS/EtOH/$H_2O$/$HNO_3$ was added drop wise into the mixture of Ca $(NO_3)_2 \cdot 4H_2O$/ $(NH_4)_2HPO_4$/ $HNO_3$ and last one with the TTiP/EtOH/acacH solution under continuous stirring for 1 hour keeping the pH at 1.

## 2.2. Structural and morphological characterization

### 2.2.1 Dynamic rheological measurement

Oscillatory shear rheological measurements were carried out using a strain controlled rheometer ARES G2 from TA Instruments on the $SiO_2$-CaO-$P_2O_5$ and $SiO_2$-CaO-$P_2O_5$-$TiO_2$ sol-gel materials. The geometry used to perform the measurements was a double concentric cylinder, with a diameter of 32 mm, made of titanium.

After preparation, a quantity of 4 mL from the studied sol was immediately investigated by rheological measurements. The quantity of the sample outlast was kept in a thermostatic bath at 37±0.1°C with the purpose of observing the macroscopic evolution of the sol-gel transition. A solvent trap was used on the top of geometry in order to minimize the eventual solvent evaporation of the sample during measurements.

In order to determine the linear viscoelastic region of the materials, oscillatory measurements at constant frequency (1Hz) and variable strain amplitude from 0.01% to 100%, was performed. The evolution of the storage G' and loss G'' modulus as function of time was then recorded at 37 °C under constant strain (0.1%), (1Hz) frequency for the $SiO_2$-CaO-$P_2O_5$ samples (4Si and 2Si) and (1%) strain, (1Hz) frequency for $SiO_2$-CaO-$P_2O_5$-$TiO_2$ (4Si-5Ti, 2Si-5Ti, 4Si-20Ti and 2Si-20Ti) respectively, recording one point every 6 minutes. In addition, oscillatory strain and frequency sweeps measurements were performed on the formed swollen network by recording 6 points per decade in oscillatory frequency sweeps and 10 points per decade in oscillatory strain sweeps.

### 2.2.2 Determination of Young's modulus by Texture Analysis

Uniaxial compression tests of $SiO_2$-CaO-$P_2O_5$ (4Si and 2Si) gels and $SiO_2$-CaO-$P_2O_5$-$TiO_2$ (4Si-5Ti and 4Si-20Ti) gels respectively were achieved with a TA.XT plus texture analyzer. The tested materials were kept in beakers; left there until gelation, being covered with parafilm in order to minimize the evaporation of the solvent. The radius of the beaker for a sample with 80 mL was about R = 0.0504 m. The tests were performed with one hour frequency until the macroscopic syneresis. Preliminary tests at different strain rates were performed in order to ensure the linear domain of the measurements. The parameters used for compression tests were then set up at 0.3 % strain and a test speed of 0.05 $mm.s^{-1}$.

The determination of gel strength was done by applying a force with a cylindrical probe onto material surface. The radius of cylindrical geometry was 0.0125 m. The Young's modulus was evaluated using the Oakenfull *et al.* method [8]. According to this approach, the measured force $F_0$ must be corrected taking into account the limited dimensions of the geometry.

The force corrected $F_c$ is given by:

$$F_c = F_0 - F_p = F_0 - [\pi \cdot \rho \cdot \delta \cdot g r^2 \cdot R^2] / [R^2 - r^2] \quad (1)$$

where $\rho$ is the density of the gel; $\delta$ the penetration distance and g the acceleration due to gravity.

An apparent Young modulus E is then deduced from the following equation:

$$F_c H = E \cdot \delta \cdot \pi \cdot r^2 \quad (2)$$

where H is the initial height of the gel.

### 2.2.3 Thermal analysis results DTA/TG

The thermal analyses were conducted on a Shimadzu type derivatographs DTG-60H (differential thermal and thermo gravimetric analyses) with a rate of 10 °C/min using approximately 10 mg of powder in the temperature range of 28-1000 °C. Alumina crucibles were used and the measurements were conducted in a dynamic nitrogen and air atmosphere at a flow rate of 70 ml/min.

### 2.2.4 Structural characterizations by X-Ray diffraction

The structural characteristics of dried powders at 100°C during 48 hours and after the annealing process at 350°C/1 hour, 550°C/1 hour and 700°C/1 hour were investigated by X-ray diffraction measurements. These analyses were performed with a Shimadzu XRD-6000 difractometer using CuKα radiation and with Ni-filter. The measurements were performed with a scan speed of 2 °/min in the 2θ range 10 - 70 º.

### 2.2.5 Structural characterizations by FTIR spectroscopy

In order to obtain more detailed information about the structural changes, FTIR study has been carried out for the dried and annealed samples at 350°C, 550°C, 700°C. The FTIR spectra for the 4Si, 2Si and 4Si-5Ti, 2Si-5Ti, 4Si-20Ti, 2Si-20Ti samples were recorded, at room temperature in the spectral range 400 - 4000 $cm^{-1}$ with a JASCO FT/IR-6200 infrared spectrometer at a resolution of 4 $cm^{-1}$ and 256 scans. A quantity of 0.8 mg of powder sample was mixed with 150 mg of KBr, compressed at 100 $N/mm^2$ to form the pellets.

### 2.2.6 Textural properties determined by BET and BJH method

Specific surface areas of the glass powders calcined at 550°C were determined from the Brunauer - Emmett - Teller (BET) equation in a relative pressure range between 0.05 and 0.4 [9]. Furthermore, the pore volume and pore diameter distribution were derived from desorption branches of the isotherms by the Barrett-Joyner- Halenda (BJH) model [10]. All isotherms are described using IUPAC nomenclature [11].

### 2.2.7 Morphological characterization by Scanning Electron Microscopy

Scanning electron microscopy (SEM) (FEI QUANTA 3D FEG dual beam) in high vacuum work mode with EDT (Everhart Thornley Detector) was used for the analysis of the microstructure and morphology of the glass powders calcined at 550°C. In order to amplify the secondary electrons signal, a cover of 5 nm thickness was performed with Pt-Pd into Agar Automatic Sputter Coater, in Ar atmosphere.

## 2.3 Bioactivity assays

As well *in vitro* tests were carried out on two classes of materials annealed at 550°C. Firstly, were tested the 2Si and 4Si samples, and then, the 2Si-5Ti, 2Si-20Ti 4Si-5Ti, 4Si-20Ti respectively. The samples were incubated in Kokubo's balanced salt solution (SBF) (Table 3) with the ionic concentration nearly equal to the human blood plasma, in static conditions [12].

**Table 3. Table of simulated body fluid, the Kokubo's balanced salt solution composition**

| Ion | Human Blood Plasma (mM) | Kokubo-SBF (mM) |
|---|---|---|
| $Na^+$ | 142 | 142 |
| $K^+$ | 5 | 5 |
| $Mg^{2+}$ | 1.5 | 1.5 |
| $Ca^{2+}$ | 2.5 | 2.5 |
| $HPO_4^{2-}$ | 1 | 1 |
| $HCO_3^-$ | 27 | 4.2 |
| $Cl^-$ | 103 | 147.8 |
| $SO_4^{2-}$ | 0.5 | 0.5 |
| Buffering agent | -- | Tris |

The incubation technique adopted consists in the glass powders immersion into SBF according to the ratio 10 mg/mL during various time periods at 37°C. The 2Si, 2Si-5Ti, 2Si-20Ti and 4Si, 4Si-5Ti, 4Si-20Ti samples, were removed after 1, 6, 24 hours and 21 days respectively. The powders immersed in SBF solution were filtered and washed with ultrapure water. Finally, in order to obtain information about the chemical reactivity of nanostructured materials after immersion, different techniques were used, namely XRD, FTIR and SEM.

# 3. RESULTS AND DISCUSSION

## 3.1 Structural and morphological characterization

### 3.1.1 Dynamic rheological measurements

A typical time dependent sol-gel behaviour of the elastic G' and viscous G'' moduli for the 4Si and 2Si samples at constant strain (0.1%) and frequency (1 Hz) is presented in Figure 1. In the initial part of the cross-linking reaction the loss modulus G'' is greater than the elastic modulus G', pointing out the liquid nature of the medium. The gelation time ($t_g$) which corresponds to the formation of an infinite aggregate [13] was evaluated by the crossover of G' and G''. The estimated $t_g$ values are presented in Table 4. They are in a good agreement with the macroscopic ones.

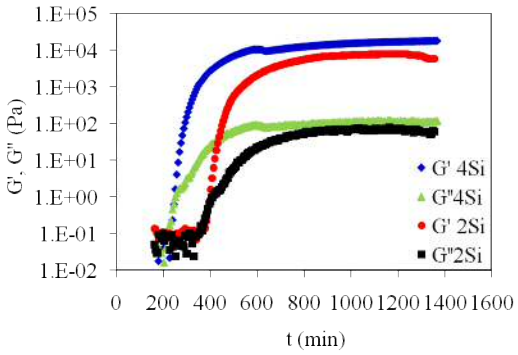


**Figure 1. Time evolution of elastic G' and viscous G" moduli of 4Si and 2Si systems at a constant strain (0.1%) and frequency (1Hz).**

**Table 4. The estimated gelation times for the studied samples**

| Sample Name | $t_g$ (min) |
|---|---|
| 4 Si | 252 ± 6.66 |
| 2Si | 408 ± 3.33 |

The same samples were kept in the rheometer for 24 hours in the case of 4Si, and 48 hours in the case of 2Si samples. Oscillatory measurements were performed using frequency and strain sweeps. Figure 2 displays the strain dependence of G' and G" moduli.

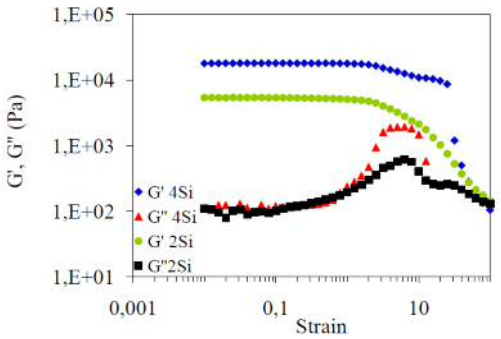


**Figure 2. Storage modulus G' and loss modulus G" versus strain amplitude measured at 1 Hz oscillation frequency of 4Si and 2Si swollen materials.**

A preliminary qualitative analysis of Figure 2 indicates a more dense structure for the 4Si sample than for the 2Si sample which is confirmed by the higher values of linear elastic modulus: 18 kPa for the 4Si sample compared to 5.4 kPa for the 2Si sample (Table 5).

**Table 5.Values of G' in the linear viscoelastic domain from strain sweeps measurements.**

| Sample Name | G' (kPa) |
|---|---|
| 4 Si | 18 ± 0.7 |
| 2Si | 5 ± 0.24 |

These results indicate that the viscoelastic properties are independent of the calcium content and probably are mainly due to the chemical bonds between the siloxane groups that form the primary clusters. This assumption is supported by a previous study [14] solid-state 29-Si nuclear magnetic resonance. It was thus demonstrated that the network of these gels was formed by siloxane bonds. Moreover, some other authors [15] pointed out that the silica species aggregate alone and form the gel framework while the calcium and phosphorus remain as soluble salts in the structure. Another interesting feature is the occurrence of a maximum of G'' with a greater amplitude for 4Si than for 2Si sample. It was proposed that this tendency of the loss modulus corresponds to structural rearrangements [16].

Additional information about the rheological behaviour of the silica-calcium-phosphate swollen gels could be obtained from the Figure 3 which presents the evolution of G' and G'' moduli as function of frequency sweeps in the range 0.01 - 10 Hz at constant strain (0.1 %).

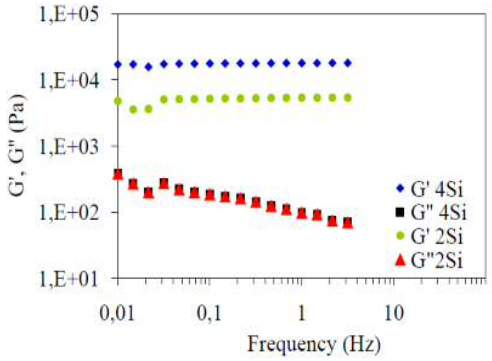


**Figure 3. Frequency dependence of storage G′ and loss G″ modulus at constant strain (0.1 %) of the studied swollen gels.**

The elastic modulus G' for both samples remains independent of the frequency whereas G" exhibits a slight decrease after 1Hz for all studied samples. These results show that a stable tridimensional network was formed and the solid behaviour was more pronounced for the highest silicon concentration (4Si). The low frequency of G" implies the existence of relaxation processes resulting from very slow structural rearrangements [16].

The influence of the modified solvent and chelating agent ratios at a given concentration of titanium alkoxide 5, 20 mol % $TiO_2$ and a constant catalyst ratio was investigated. The typical time dependent curves were recorded from the initial sol state until the final gel and are presented in Figure 4 (a)-(d).

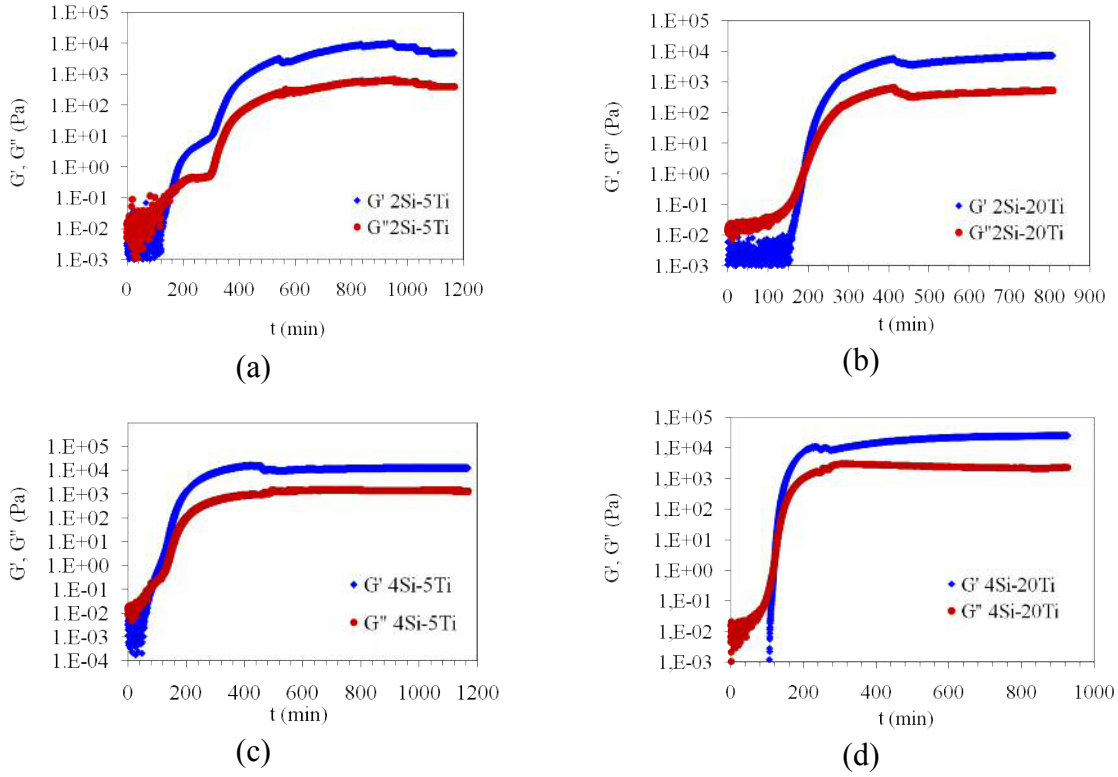


**Figure 4. Time evolution of the elastic G' and viscous G" moduli of (a) 2Si-5Ti, (b) 2Si-20Ti and (c) 4Si-5Ti, (d) 4Si-20Ti systems at a constant strain (1%) and frequency (1Hz).**

In the initial part of the cross-linking reaction, the loss modulus G'' is greater than the elastic modulus G', pointing out the liquid nature of the medium. The estimated $t_g$ values are presented in Table 6. As can be seen, the aggregation process is faster for the sol with higher silicon content (4Si-5Ti, 4Si-20Ti) and smaller concentration of calcium. In addition, these findings are supported by other literature reports [17] were with neutron small-angle scattering (SAS) and dynamical rheometry techniques it was shown that the decrease in calcium concentration induces an increase of the gelation time.

**Table 6. Estimated gelation times of the studied samples**

| **% Ti** | **5** | **20** |
|---|---|---|
| **4 Si**<br>**$t_g$ (min)**<br>**2Si** | 90 ± 1.37 | 121 ± 0.33 |
| **$t_g$ (min)** | 159 ± 1.13 | 189 ± 0.71 |

Figure 5 displays the strain dependence of G' and G" moduli between 0.01% and 100 % at a constant frequency of 1Hz. A preliminary qualitative analysis of these curves indicates a more dense structure for the 4Si-20Ti sample than for 4Si-5Ti sample.

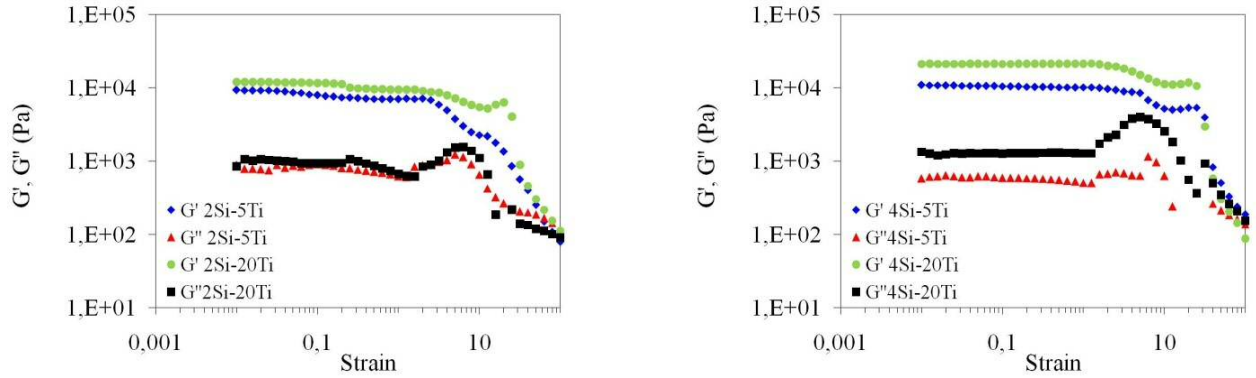


(a) (b)

**Figure 5. Storage modulus G' and loss modulus G" versus strain amplitude measured at 1 Hz oscillation frequency of: (a) 2Si-5Ti, 2Si-20Ti and (b) 4Si-5Ti, 4Si-20Ti swollen materials.**

The estimated values of the linear elastic modulus are presented in Table 7.

**Table 7. Values of elastic G' modulus in the linear viscoelastic domain performed in strain sweeps tests.**

| **% Ti** | **5** | **20** |
|---|---|---|
| 4 Si<br>**G' (kPa)** | 10 ± 0.17 | 21 ± 0.1 |
| 2 Si<br>**G' (kPa)** | 3 ± 0.32 | 10 ± 0.73 |

These results indicate that the viscoelastic properties are mainly based on the chemical bonds between the siloxane groups that form the primary clusters because the reactivity of titanium alkoxide was reduced by acacH. Indeed, this assumption was confirmed in a previous study [14] by solid-state 29-Si nuclear magnetic resonance. Also, the increase of condensation rates of titanium precursor induce the deprotonation of the hydroxo ligands in the alkaline earth conditions, where strong nucleophilic interactions are produced [18]. Another interesting feature is the occurrence of a maximum of G" with a greater amplitude for 4Si-20Ti than for 2Si-20Ti sample. It was proposed that this behaviour of loss modulus correspond to structural rearrangements (Figure 5 (a)-(b)) [19]. It was assumed that the cluster suspension undergoes a liquid to solid-like transition where the particle concentration increases by losing the free volume and the elastic modulus values are independent of the applied frequency [20].

Figure 6 displays the rheological behaviour of the silica-calcium-phosphate materials containing titanium dioxide as function of frequency sweeps in the range 0.01 - 100 Hz at constant strain (1%).

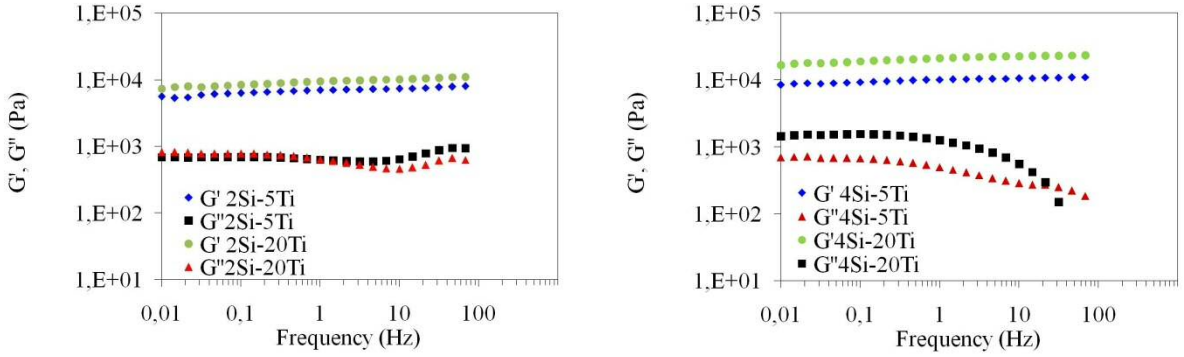


**Figure 6. Frequency dependence of storage modulus G′ and loss modulus G″ at constant strain (1%) of the: (a) 2Si-5Ti, 2Si-20Ti and (b) 4Si-5Ti, 4Si-20Ti swollen gels (23 hours).**

The estimated values of the elastic modulus in the linear domain are presented in Table 8.

**Table 8. Estimated linear domain of elastic G' modulus in the frequency sweeps measurements.**

| **% Ti** | **5** | **20** |
|---|---|---|
| 4 Si **G' (kPa)** | 9 ± 0.88 | 20 ± 0.73 |
| 2 Si **G' (kPa)** | 6 ± 0.75 | 9 ± 0.21 |

By inspecting the loss modulus G'' for all samples, one can observe a slight decrease after 10 Hz for the 4Si-20Ti sample and after approximately 100 Hz for the 4Si-5Ti sample. This behaviour implies the existence of some relaxation processes resulting from the very slow structural rearrangements [16].

In terms of kinetic effect, it was found that the highest silicon alkoxide content and the smaller concentration of calcium are decreasing the $t_g$. Meanwhile, the peaks intensities from strain sweeps tests are gradually enhanced with the increase of titanium content, from 5 to 20 mol % (Figure 5 (a-b)). It has to be mentioned that the elastic modulus was enhanced for the samples containing 20 mol % of titania. Slower relaxation processes were observed for the samples with high calcium content, namely 2Si-5Ti and 2Si-20Ti.

## 3.1.2 Determination of Young's modulus by Texture Analysis

The time evolution of the Young's modulus deduced from the slope of the linear variation of the corrected force is shown in Figure 7 for the 4Si and 2Si studied samples.

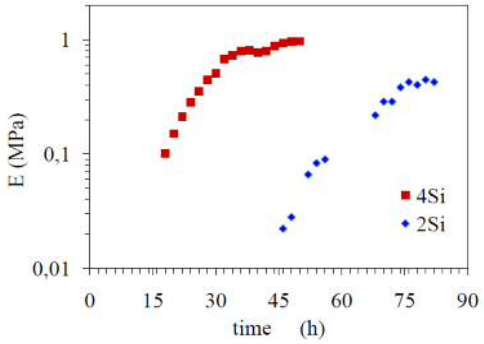


**Figure 7. Time evolution of the Young's modulus of the two studied silica - calcium - phosphate gels.**

A fast increase of Young's modulus was firstly observed in the first 38 hours for 4Si and 75 hours for 2Si followed by a slowly increase. Finally, Young's modulus tend to nearly constant values (970 kPa for the 4Si and 425 kPa for the 2Si gels) highlighting that chemical reactions are almost completed. For longer testing times, the macroscopic syneresis was observed to inducing the decrease of Young's modulus. Moreover, an increase of the Young's modulus for 4Si-5Ti gel was observed until 17 hours, whereas for 4Si-20Ti sample until 21 hours, which was followed by a slowly decrease (Figure 8).

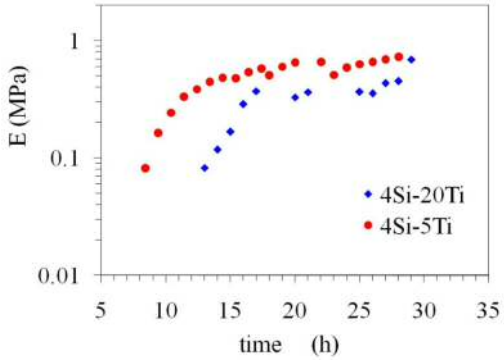


**Figure 8. Time evolution of the Young's modulus of the two studied silica - calcium - phosphate with titanium dioxide gels.**

The smaller amount of titanium alkoxide strongly influences the texture of gels while a denser network can be related to the 4Si-20Ti material.

## 3.1.3 Thermal analysis results DTA/TG

Figure 9 (a)-(b) presents the DTA-TGA curves recorded for the 4Si and 2Si samples, dried at 100 °C.

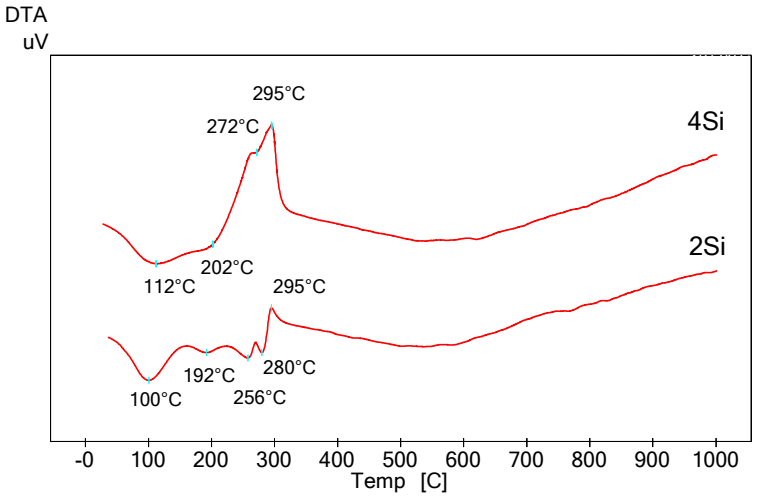


(a)

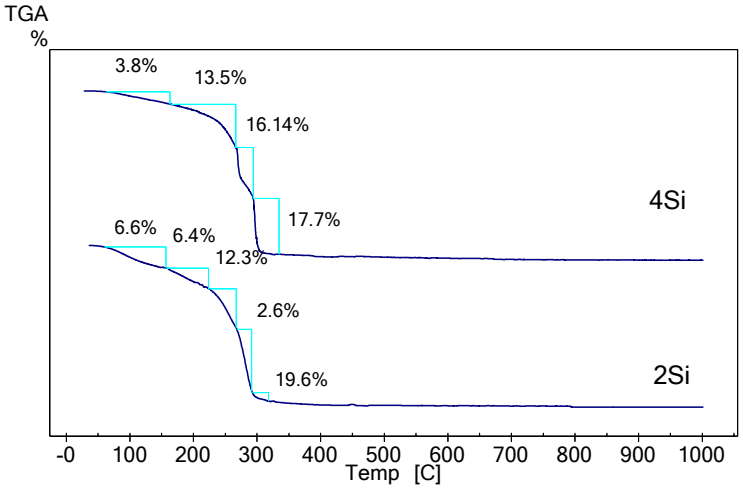


(b)

**Figure 9. Thermal curves of 2Si & 4Si dried samples: (a) DTA and (b) TGA.**

Generally, the aqueous solutions of ammonium nitrate undergo a double decomposition reaction with metal salts, $NH_4NO_3$ acting as an oxidizing agent in aqueous solutions by reducing various metals at ambient temperatures [21]. Taking into account the large amount of ammonium used in the performed chemical reactions, the following effects can be predicted and associated with the following processes:

- the first high amplitude endothermic peak around θ ~100°C (for 2Si) and θ ~112°C (for 4Si) corresponds to ~6.6 % mass loss and ~3.8 % respectively due to the surface dehydration of the materials and to water elimination resulted from the reaction of the ammonium hydroxide $NH_4OH$ [21]. Based on XRD, FTIR and DTA literature investigations, [22] at θ ~105 °C two moles of calcium phosphate dehydrate are combined in order to eliminate one mole of water. The remaining three moles of water were lost at θ ~165 °C with the formation of $Ca_2P_2O_7$.
- the second endothermic peak at θ ~ 202 ºC (4Si) and θ ~192 ºC (2Si), with a mass loss of ~ 13.5 % and

6.4 % was associated with a structural transformation of $NH_4NO_3$, shifted here to higher temperature as compared to data reported in literature [23]:

- an overlapping of events occurs in the temperature range θ ~ 256-280 ºC; the small endothermic peak at θ ~ 256 ºC (present for the 2Si sample) could be related to the thermal decomposition of $NH_4NO_3$
- the endothermic signals at θ ~ 280 ºC (2Si) and θ ~ 272 ºC (4Si) are due to the dehydration of calcium phosphate [24, 25]. Moreover, the dehydration of calcium hydrogen phosphate presents a theoretical mass loss estimated at 20.93% [26]. Our results show an experimentally mass loss of ~ 22.2 % that occurs in the temperature range θ of 280 - 295 °C for the 2Si sample.
- the high exothermic peaks at θ ~ 295 °C for the 4Si and for the 2Si samples are due to the decomposition of the un-reacted residual organic compounds. Afterwards, the samples mass remains constant over the whole investigated temperature range.

The DTA/TG signals recorded at a heating rate of 10 °C/min for the 2Si-5Ti, 2Si-20Ti, 4Si-5Ti, 4Si-20Ti gel specimens dried at 100 °C during 24 hours, are displayed Figure 10 (a)-(b).

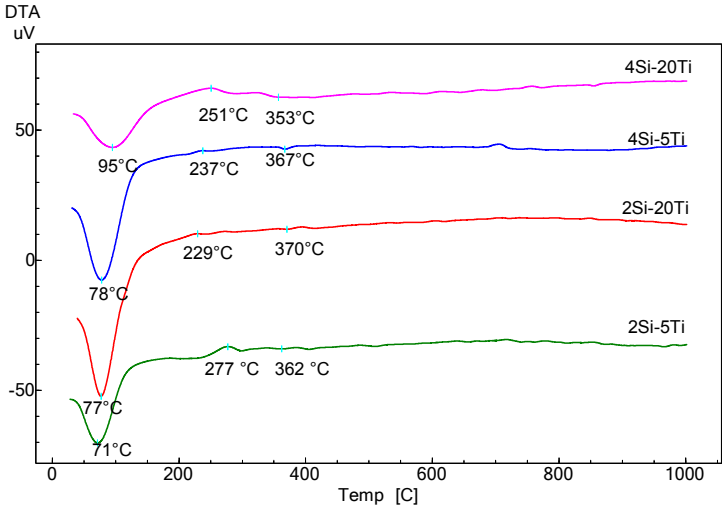


(a)

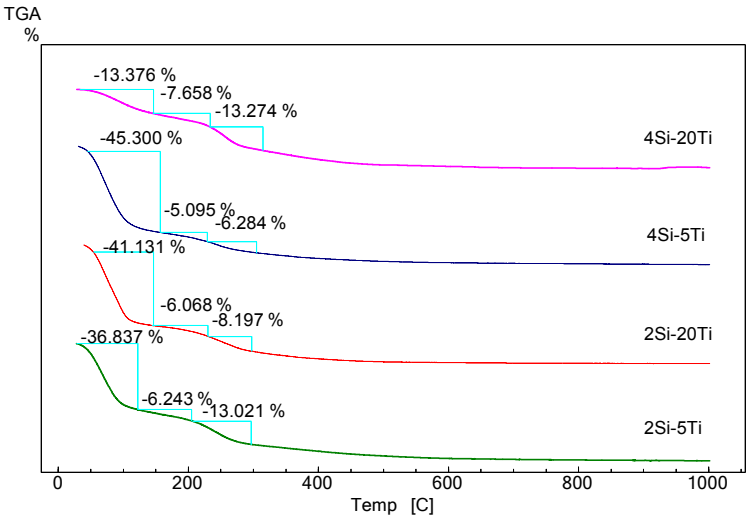


(b)

**Figure 10. DTA curves: (a) DTA curves of dried 2Si-5Ti, 2Si-20Ti and 4Si-5Ti, 4Si-20Ti gels at a heating rate of 10 °C/ min. (b) TGA profile of 2Si-5Ti, 2Si-20Ti and 4Si-5Ti, 4Si-20Ti dried samples.**

The weight losses of the studied samples accompanied by the endothermic and exothermic events are presented in Table 9.

**Table 9. Data from TGA curves of 4Si-5Ti, 4Si-20Ti and 2Si-5Ti, 2Si-20Ti.**

| ***Sample Name*** | ***Air and $N_2$ atmosphere peak Exo/Endo*** | | | **Events temperature (°C)** | **Total weight losses(%)** |
|---|---|---|---|---|---|
| ***2Si-5Ti*** | endothermic | exothermic | endothermic | 71, 277, 362 | **56.10** |
| ***2Si-20Ti*** | endothermic | exothermic | endothermic | 77, 229, 370 | **55.40** |
| ***4Si-5Ti*** | endothermic | exothermic | endothermic | 78, 237, 367 | **56.68** |
| ***4Si-20Ti*** | endothermic | exothermic | endothermic | 95, 251, 353 | **34.30** |

- the first broad endothermic effect in the range θ ~71°C and θ ~95°C is due to interstitial water elimination and to organic solvent (ethanol) removal. Ragai's *et al.* studies showed the existence of three kinds of water bonded to titania particles which give three endothermic peaks in the range θ ~ 94-107°C, θ ~350-500°C respectively [27]. These peaks correspond to interstitial water, coordinative bounded water and rigidly bounded water due to hydroxyls ions that we supposed to be of type Si-OH, Ti-OH species [28].
- thereafter, the second exothermic peak in the range of temperature θ ~ 250 ºC and θ ~275 ºC, is probably caused by ignition of the already released acetylacetone vapors, as compared to data reported in literature [28] and to thermo-oxidative degradation of the organic matter.

- the third endothermic signal at θ ~ 365-371 ºC can be ascribed to physisorbed water supported by the existence of some amount of chemically bounded water [29]. Afterwards, the further weight loss is probably due to the densification process of amorphous powders until their crystallization.

## 3.1.4 Structural characterizations by X-Ray diffraction

The XRD patterns of the 2Si and 4Si samples after different heat treatments are shown in Figure 11(a)-(b).

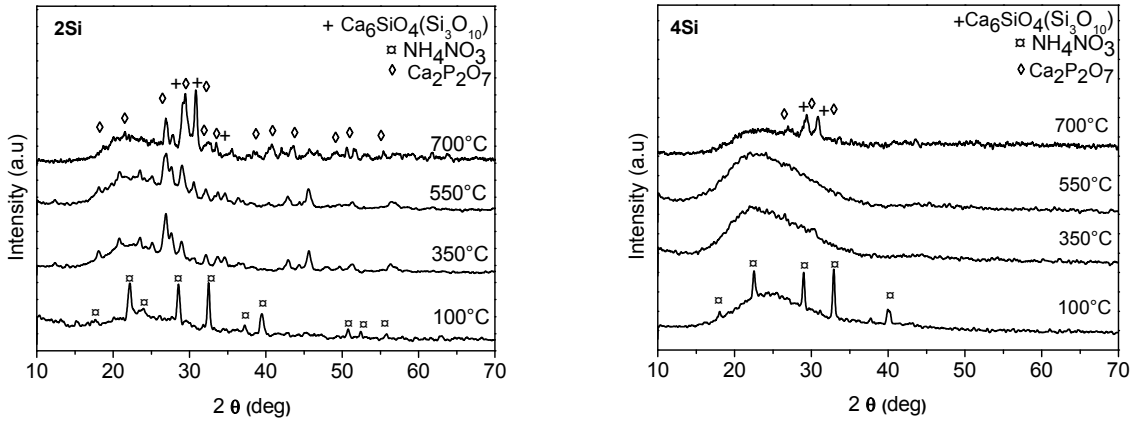


(a) (b)

**Figure 11. XRD patterns of samples heated at 100°C, 350°C, 550°C, 700°C: (a) 2Si, (b) 4Si.**

The XRD patterns for the 4Si and 2Si samples after being dried at 100˚C exhibit similar peaks (Figure 11 (a)-(b)), corresponding to un-reacted ammonium nitrate $NH_4NO_3$ phases (PDF card 08-0452)[30]. Moreover, the samples with high $SiO_2$ content (4Si) denote a non-crystalline structure after thermally treatments at 350 and 550°C, reflected by the broad 2 θ diffraction peak recorded between 20 and 30° (see Figure 11 (b)) [31, 32]. The 4Si sample presents a $Ca_2P_2O_7$ phase (PDF card 09-0346) besides an amorphous matrix at 700°C. Afterwards, the XRD patterns at 350°C for the 2Si sample (Figure 11 (a)) revealed that the nitrate component disappears and the amorphous silica-based network decomposes into a calcium pyrophosphate ($Ca_2P_2O_7$) phase. The presence of $Ca_2P_2O_7$ and that of a small amount of calcium silicate phases (kilchoanite $Ca_6SiO_4Si_3O_{10}$) (PDF card 29-0370) were observed at 700 ºC. Concerning the structural characteristics, the samples having the general formula $(CaO)_x(SiO_2)_{1-x}$ have been proved to possess significant potential as bioactive bone-regenerative materials, since they exhibit *Class A* bioactivity [33].

The XRD patterns for the 2Si-5Ti, 2Si-20Ti and 4Si-5Ti, 4Si-20Ti samples after drying at 100°C and annealed at 350°C, 550°C, 700°C respectively are shown in Figure 12 (a)-(d). The data emphasise the predominant amorphous state until 550°C; therefore the hydrolyzed $TiO_2$ was not precipitated during the

synthesis.

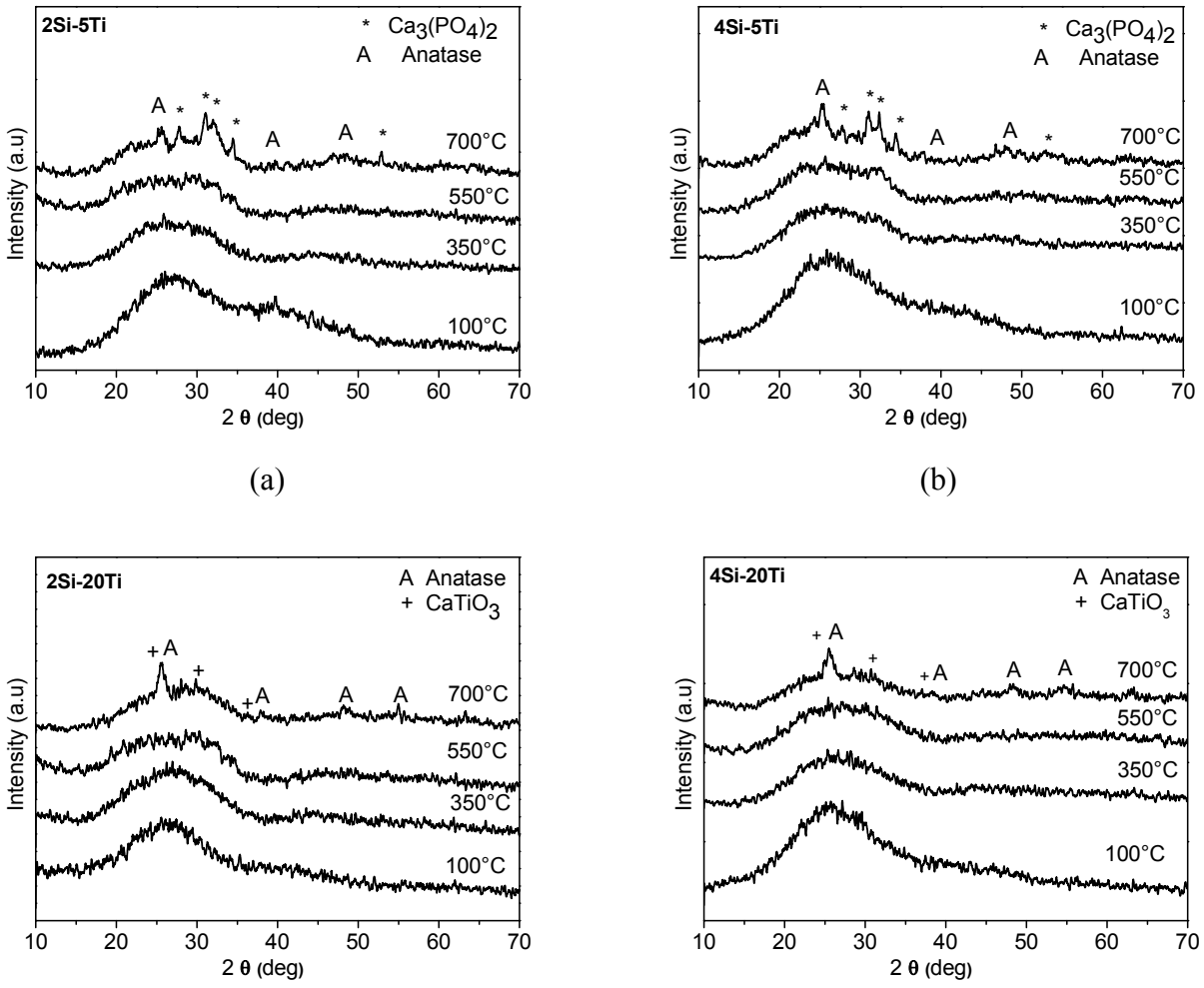


**Figure 12. XRD patterns of dried and calcined samples at 100°C, 350°C, 550°C, 700°C: (a) 2Si-5Ti, (b) 4Si-5Ti, (c) 2Si-20Ti and (d) 4Si-20Ti.**

Moreover, by increasing the thermal treatment at 700°C, one can observe from the XRD patterns that the samples with lower $TiO_2$ content present anatase (PDF card 21-1272) and calcium phosphate ((Whitlockite $Ca_3(PO_4)_2$) (PDF card 09-0169) crystalline phases, beside an amorphous silica matrix. The samples with the highest concentration of $TiO_2$ present two types of crystalline phases, beside an amorphous matrix. The reflection peaks consist in anatase (PDF card 21-1272) and calcium titanium oxide $CaTiO_3$ (PDF card 39-0145) phases, beside an amorphous matrix.

## 3.1.5 Structural characterizations by FTIR spectroscopy

The FTIR spectra of the 4Si and 2Si are presented in Figure 13 (a)-(b) evaluating the structural changes that occur during subsequent heat treatments.

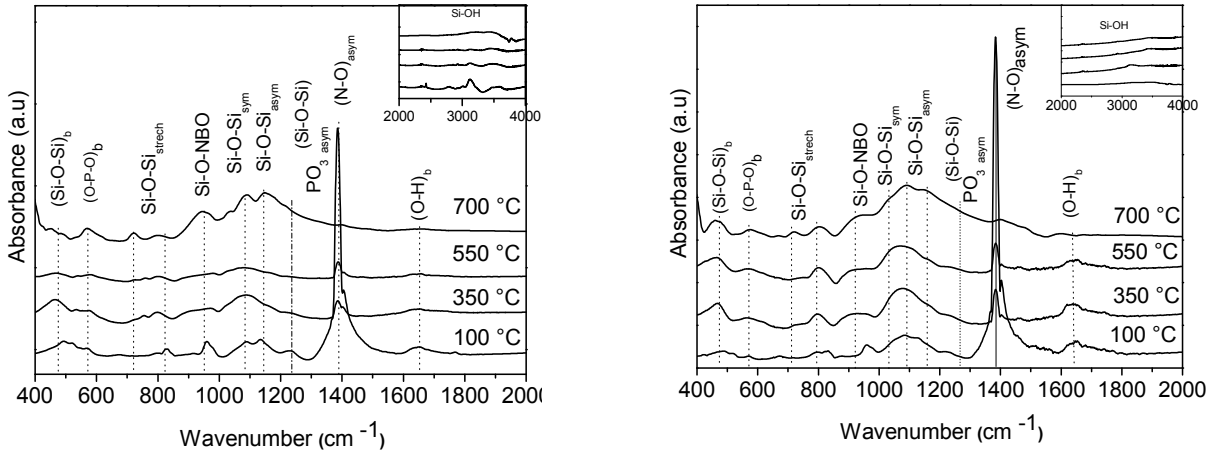


**Figure 13. Fourier transform infrared absorption spectra of the glass samples after heat treatment at 100 °C, 350, 550°C, 700°C: (a) 2Si (b) 4Si. The inset shows the spectral domain between 2000 - 4000 cm$^{-1}$.**

Table 10 presents the results concerning the main FTIR frequencies and assignments of the 2Si and 4Si but also of the materials 2Si-5Ti, 2Si-20Ti 4Si-5Ti, 4Si-20Ti.

**Table 10. Frequencies and assignments of IR absorption bands for the spectra shown in Fig. 13 and 14.**

| Observed bands (cm$^{-1}$) | Assignments |
|---|---|
| 1620-1650 | deformation vibration of O-H [34] |
| 1380-1400 | asymmetric vibration of nitrate [34] |
| 1231-1200 | longitudinal optical Si-O-Si stretching vibration and asymmetric stretching of $PO_3$ groups [35] |
| 1147-1032 | Si-O-Si asymmetric stretching mode |
| 950-920 | Si-O-NBO [36]<br>Ti-O-Si stretching modes [37] |
| 800-714 | Si-O-Si symmetric stretching vibration [38] |
| 700 | P-O-P linkages in polymeric systems [39] |
| 650 | Ti-O-Ti symmetric stretching vibrations [40] |
| 525-630 | O-P-O bending mode of crystalline phosphate [41] |
| 470 | Si-O-Si bending [38] |

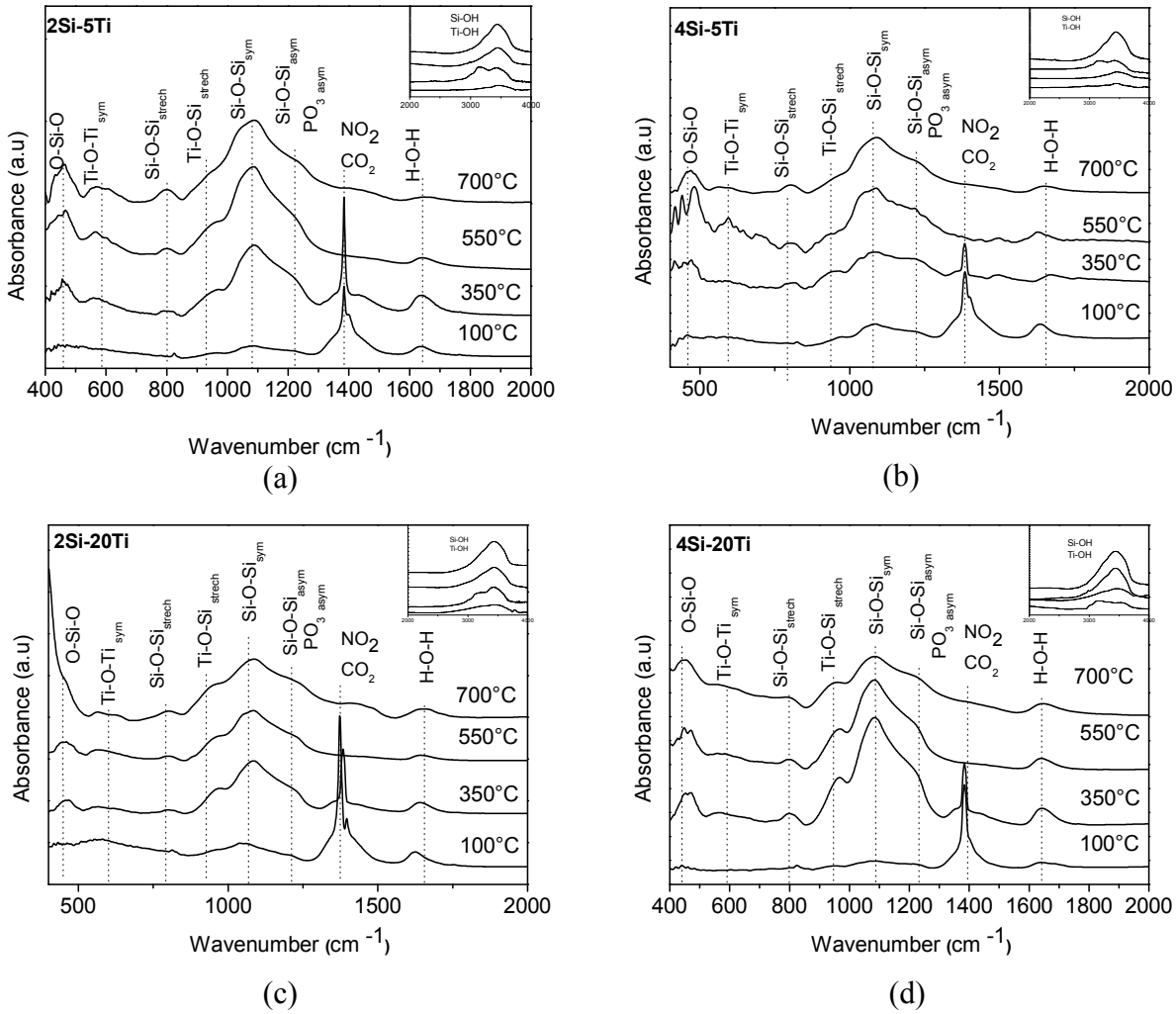


**Figure 14. Fourier transform infrared absorption spectra of the glass samples after drying at 100 °C and heat treatment at 350°C, 550°C, 700°C: (a) 2Si-5Ti, (b) 4Si-5Ti, (c) 2Si-20Ti, (d) 4Si-20Ti. The inset shows the spectral domain between 2000 - 4000 cm$^{-1}$.**

## 3.1.6 Textural properties determined by BET and BJH method

The nitrogen adsorption-desorption isotherms (Figure 15 (a)) for 2Si thermally treated samples at 550º C were identified as type IV isotherms with hysteresis loops of H4 type associated with slit-shaped pores. The 4Si sample (Figure 15 (b)) presents type IV isotherms with H2 hysteresis loops associated with ink-bottle pores [11]. By comparing the two studied samples (4Si, 2Si) one observes that once with the increase of silica content in the matrix, the surface area and pore volume increase also (Table 11).

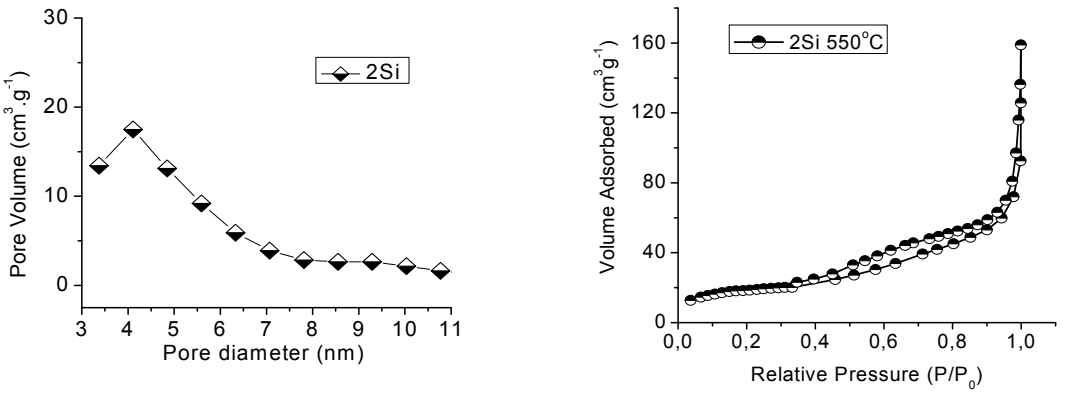


(a)

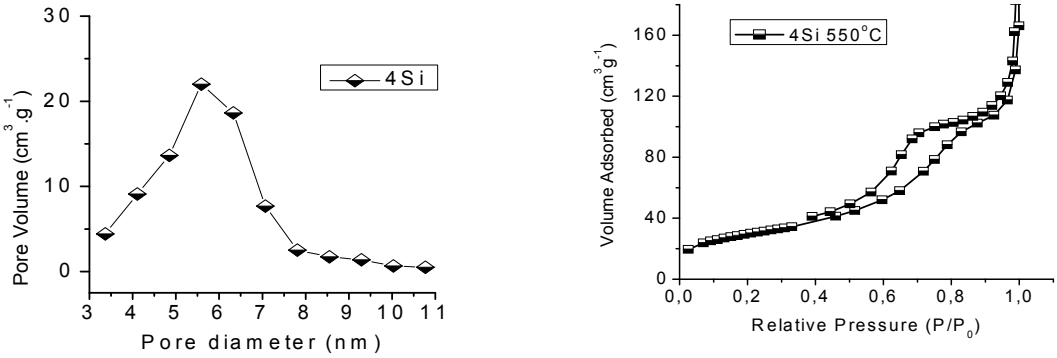


(b)

**Figure 15. $N_2$ adsorption-desorption isotherms of 2Si (a) and 4Si (b) samples thermally treated at 550° C.**

**Table 11. Textural properties of 2Si, 4Si samples thermally treated at 550°C.**

| ***Sample Name*** | ***Pore volume ($cm^3/g$)*** | ***BJH median pore diameter (nm)*** | ***BET Surface area ($m^2/g$)*** |
|---|---|---|---|
| ***2Si*** | 0.0926 | 5.5243 | 65.734 |
| ***4Si*** | 0.1801 | 6.0101 | 107.66 |

For a better understanding of titanium dioxide distribution in the silica-based matrix, textural analyses were also performed. The adsorption-desorption isotherms of the 2Si-5Ti, 2Si-20Ti and 4Si-5Ti, 4Si-20Ti samples annealed at 550°C are shown in Figure 16 (a)-(d). The 2Si-5Ti, 4Si-5Ti samples have similar type VI isotherms, associated with layer-by-layer adsorption on a highly uniform surface pores. Moreover, it is observed that the 2Si-20Ti and 4Si-20Ti samples present a type IV isotherm [11].

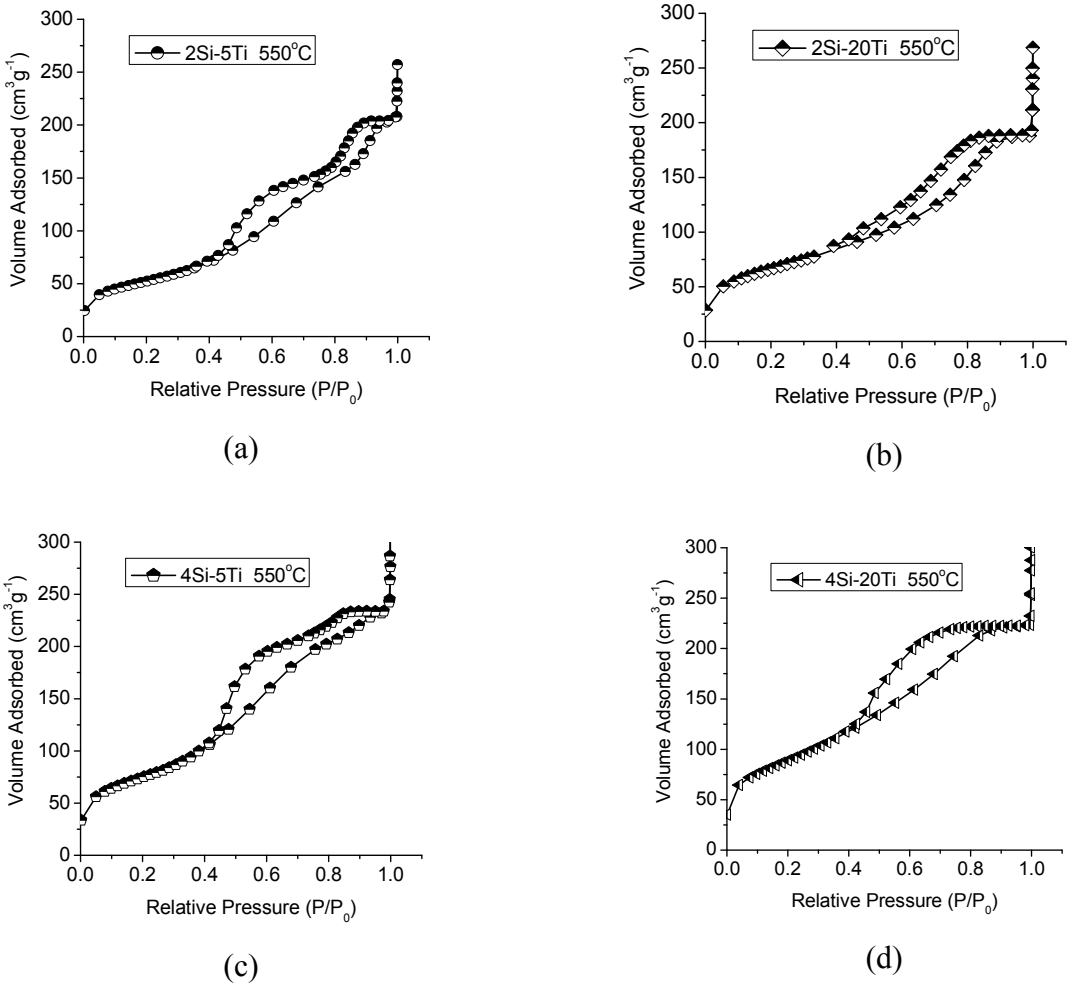


**Figure 16. Nitrogen adsorption isotherms of: (a) 2Si-5Ti, (b) 2Si-20Ti and (c) 4Si-5Ti, (d) 4Si-20Ti samples.**

The 2Si-5Ti and 2Si-20Ti samples show H1-type isotherm corresponding to bi-modal size distribution of open-ended tubular pores [39]. Additionally, by increasing the silicon oxide content one can observe (Figure 16 (c)-(d)) that the hysteresis loop changes from H1-type to H2-type, the latter being characteristic to ink bottle-like pores. Moreover, a progressive increase of specific surface area was observed by increasing the $TiO_2$ content (from 187.28 to 320.95 $m^2/g$).

**Table 12. Physico-chemical properties of the 2Si-5Ti, 2Si-20Ti, 4Si-5Ti, 4Si-20Ti samples.**

| ***Sample Name*** | *Cumulative pore volume ($cm^3/g$)* | *BJH median pore radius (nm)* | *BET Surface area ($m^2/g$)* |
|---|---|---|---|
| ***2Si-5Ti*** | 0.3306 | 4.6615 | 187.28 |
| ***2Si-20Ti*** | 0.243 | 6.2002 | 242.17 |
| ***4Si-5Ti*** | 0.2932 | 4.0329 | 266.59 |
| ***4Si-20Ti*** | 0.3643 | 4.2607 | 320.95 |

The variation of pores size distribution is further evidenced by pore size distribution curves (Figure 17). The results confirmed that the pores are in the mesopore range [11].

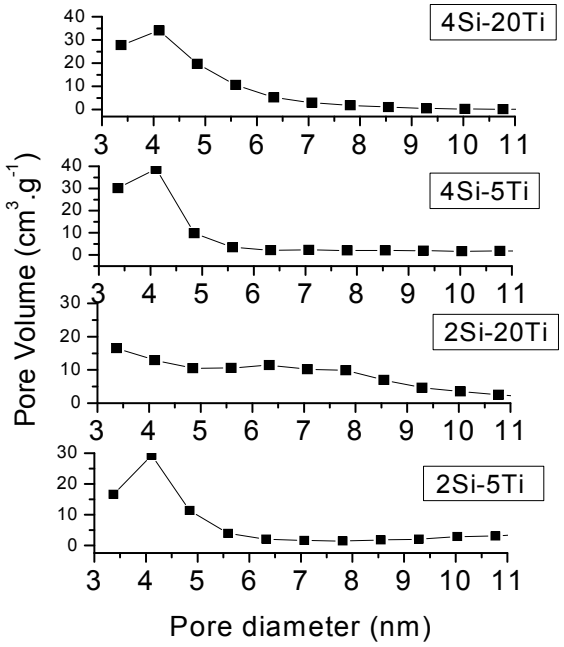


**Figure 17. Pore size distribution curves calculated by BJH method from the absorption-desorption branch of isotherms for (a) 2Si-5Ti, (b) 2Si-20Ti, (c) 4Si-5Ti, (d) 4Si-20Ti samples.**

## 3.1.7 Morphological characterization by Scanning Electron Microscopy

The SEM images of the 2Si sample (Figure 18 (A)) consist of acicular morphologies representing the calcium pyrophosphate and some calcium silicate as mentioned also by XRD analysis. For samples with higher concentration of $SiO_2$ (4Si) (Figure 18 (B)) were observed rough spherical morphologies.

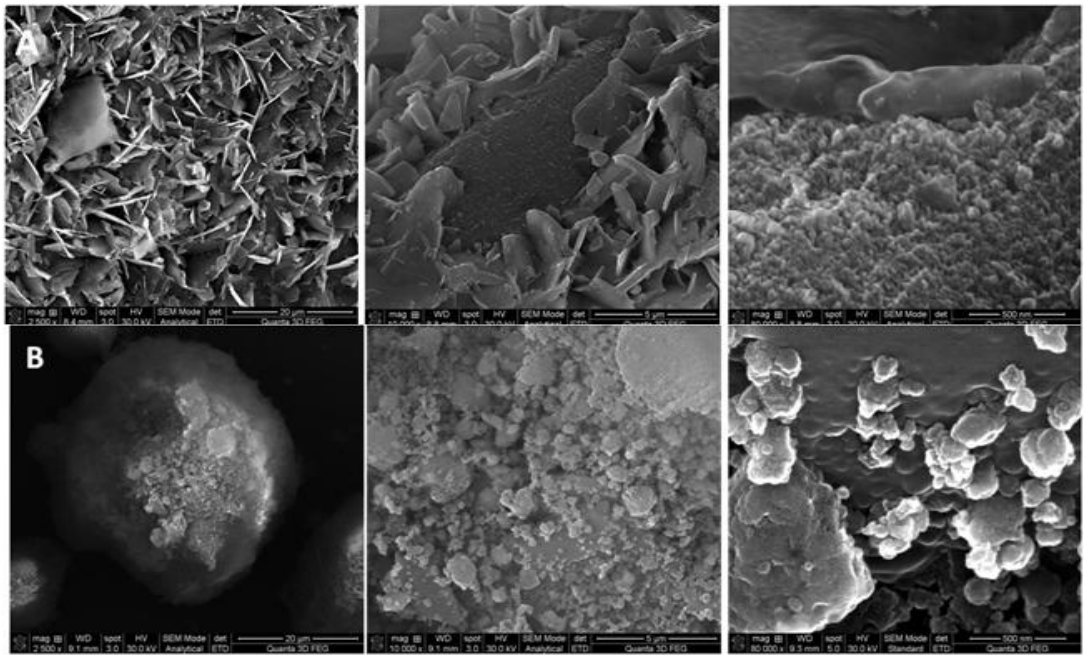


**Figure 18. SEM images of samples thermally treated at 550°C: (A) 2Si; (B) 4Si.**

Figure 19 shows the SEM images recorded for the 2Si-5Ti, 2Si-20Ti, 4Si-5Ti and 4Si-20Ti glasses annealed at 550°C. The surface of the samples appears to be rough, composed by spherical particles of about a few nanometers.

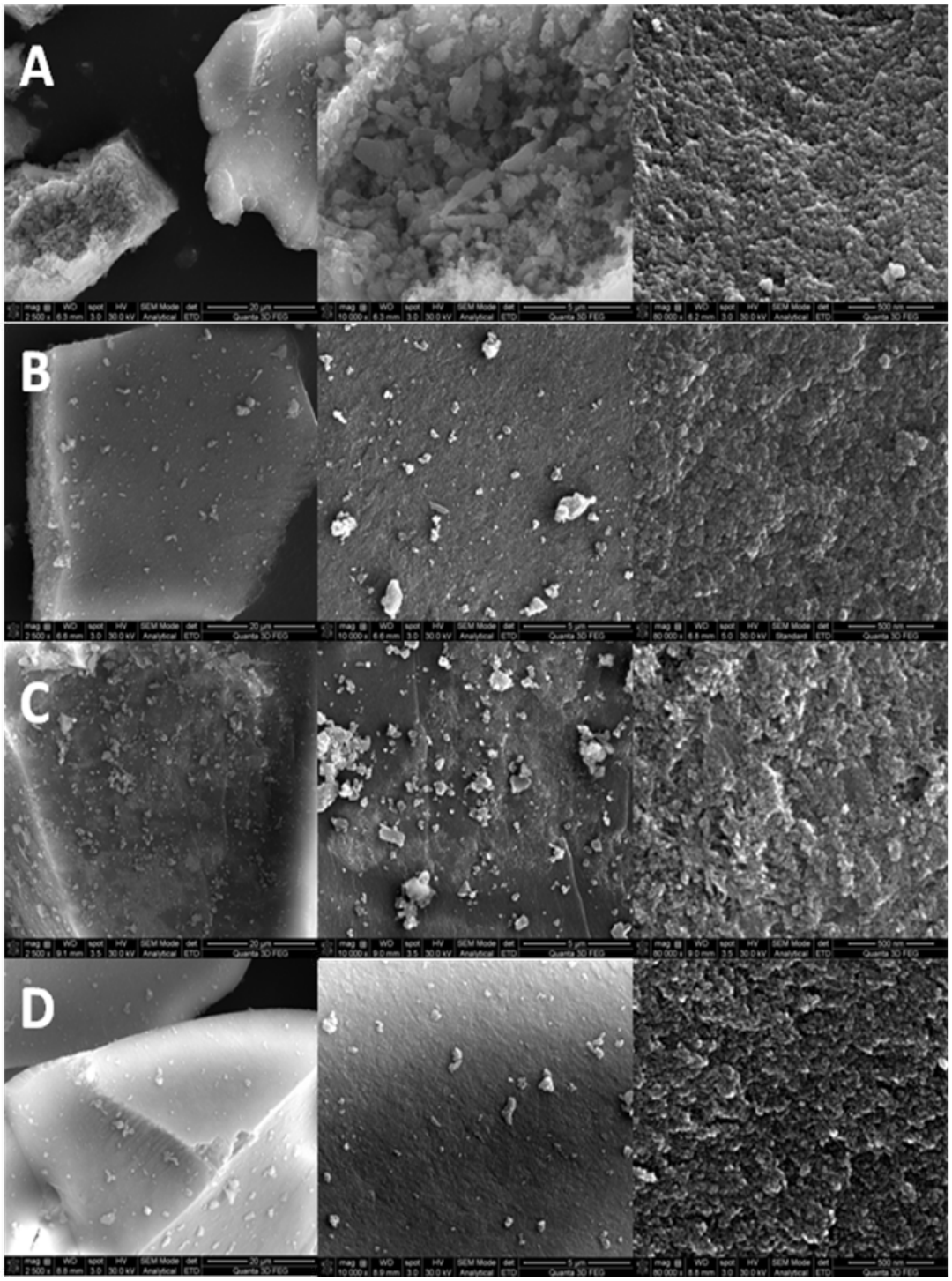


**Figure 19. SEM images of the microstructure after heat treatment at 550°C: (A) 2Si-5Ti, (B) 2Si-20Ti, (C) 4Si-5Ti, (D) 4Si-20Ti.**

## 3.8 Bioactivity assays

The XRD patterns of the 550°C thermally treated 2Si and 4Si samples after SBF immersion are displayed in Figure 20.

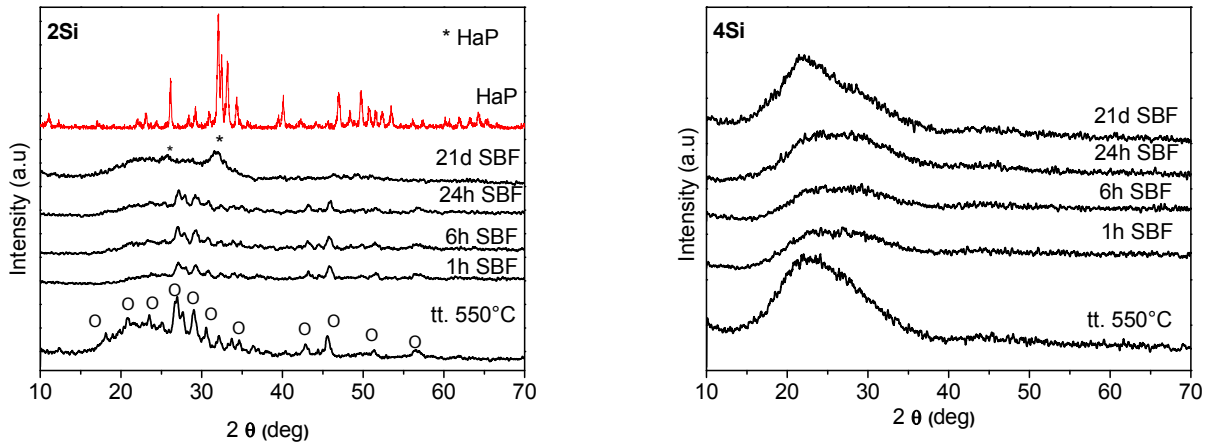


(a) (b)

**Figure 20. XRD patterns for 2Si (a) and 4Si (b) samples heated at 550°C and after 21 days of SBF incubation. For better comparison, the hydroxyapatite pattern (red spectrum) was also inserted in the figure.**

Figure 20 (a) shows a calcium pyrophosphate $Ca_2P_2O_7$ crystalline phase for the thermally treated sample at 550°C on an amorphous matrix. Furthermore, the recorded XRD patterns for up to 21 days SBF for the soaked 2Si samples revealed the presence of the new peaks located at 2θ of 26 and 32 degree. These new peaks corresponds to (002) and (211) reflection of hydroxyapatite phase (PDF card 09-0432, JCPDS). In order to clearly distinguish the hydroxyapatite phase, a standard pattern was inserted in Figure 20 (a). The 4Si sample (Figure 20 (b)) after 21 days of immersion presents a broad peak between 20 and 30 2θ degree which is probably due to small crystals formed beside the amorphous matrix.

In Figure 21 (a)-(b)) are presented the 2Si-5Ti, 4Si-5Ti samples with up to 21 days of soaking in SBF.

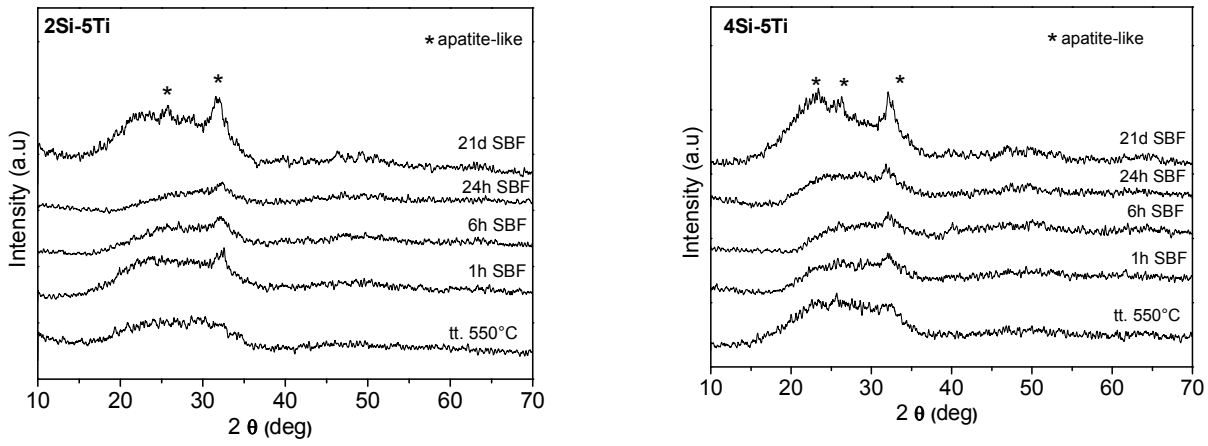


(a) (b)

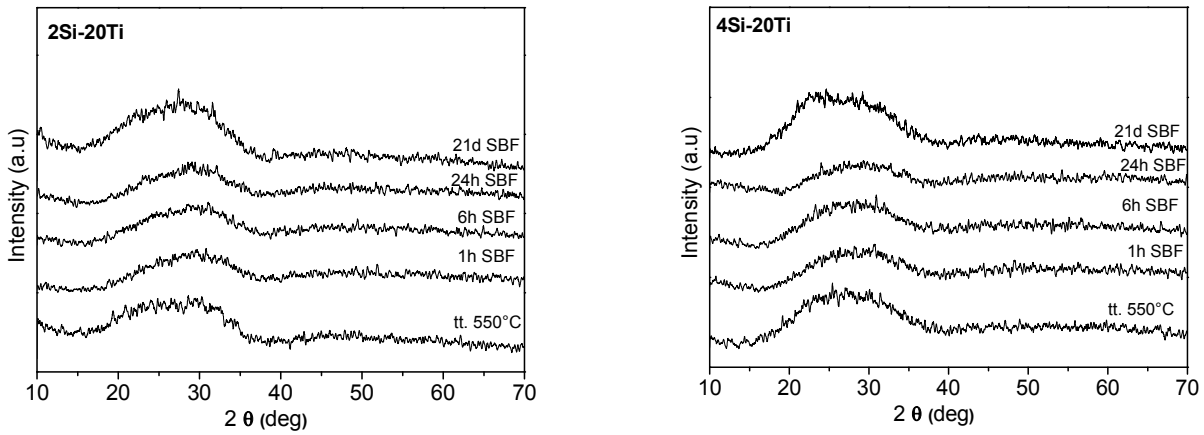


(c) (d)

**Figure 21. XRD patterns of the 2Si-5Ti, 4Si-5Ti and 2Si-5Ti, 4Si-5Ti samples heated at 550°C and immersed 21 days in SBF.**

The XRD patterns of these samples reveal the presence of apatite crystalline phases. Among these, the 4Si-20Ti samples after 21 days of incubation (see Figure 21 (d)) show a prevalent amorphous state with poor nanometric crystal size.

FTIR spectra of the 2Si and 4Si samples annealed at 550°C were displayed in Figure 22 ((a)-(b)).

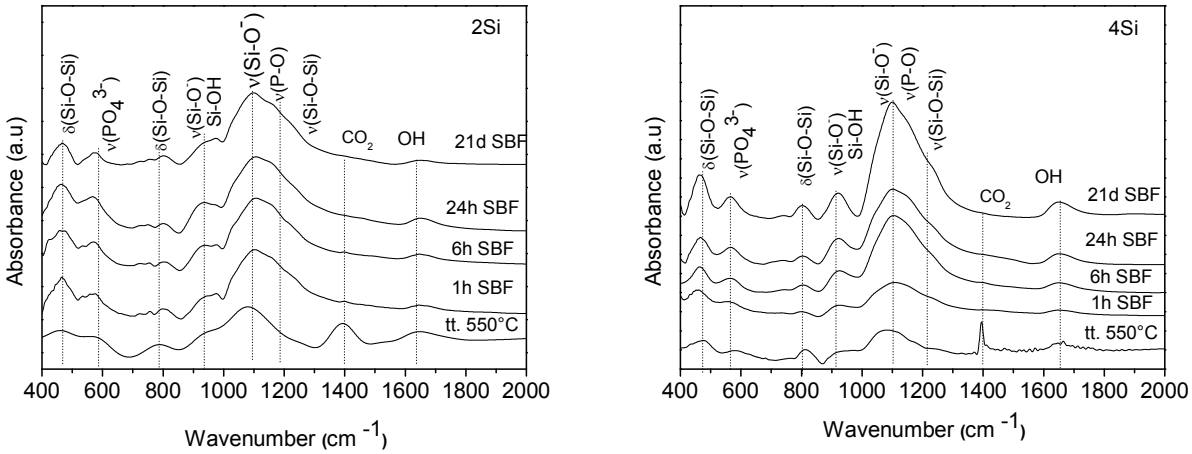


(a) (b)

**Figure 22. FTIR spectra of the glass samples with selected soaking periods (from 1hour to 21 days) in SBF: (a) 2Si; (b) 4Si.**

The FTIR spectra (see Figure 22 (a)-(b)) are dominated by strong bands, associated with vibrational modes of the $SiO_4$ and $PO_4$ tetrahedras which are overlapped. The shoulder at 1225 $cm^{-1}$ is ascribed to the longitudinal optical Si-O-Si stretching mode [42]. Moreover, the band situated at 1080 $cm^{-1}$ is attributed to the stretching vibration of $Si\text{-}O^-$ bonds [43].

After immersion in SBF from 1 hour until 21 days the band at about 1040 $cm^{-1}$, gradually increases being identified as P-O stretching mode from the $PO_4^{3-}$ groups present in hydroxyapatite [39]. Further, the shoulder at 950 $cm^{-1}$ is due to the vibration of two non-bridging oxygen atoms in the Si-O-NBO environment,

increasing over immersion time [41]. The Si-OH groups (960 $cm^{-1}$) were overlapped over the bands ascribed to $Si-O^-$ groups [39]. The band located around 800 $cm^{-1}$ is assigned to the bending motion of oxygen atoms along the bisector of the Si-O-Si bridging group [42]. A large band corresponding to P-O asymmetric bending vibrations in the $PO_4$ tetrahedra was observed at 569 and 605 $cm^{-1}$ [46]. Another strong band was also observed at 466 $cm^{-1}$, being ascribed to rocking motion of the bridging oxygen atoms perpendicularly to the Si-O-Si plane [39].

The FTIR spectra of the 4Si-Ti, 2Si-5Ti, 4Si-20Ti and 2Si-20Ti glasses after 1 hour to 21 days of immersion in SBF are presented in Figure 23 (a)-(d).

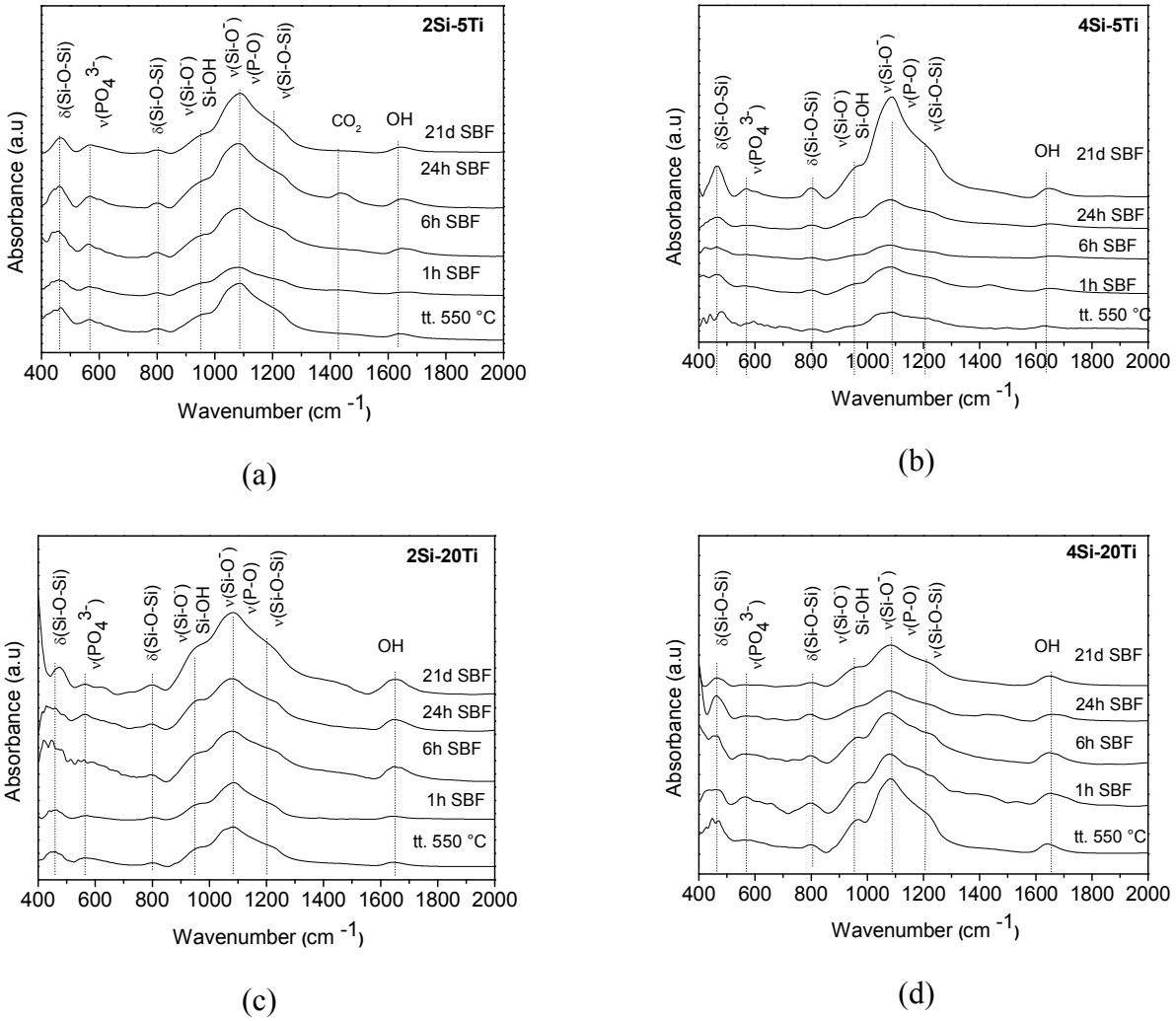


**Figure 23. FTIR spectra of the glass samples with selected soaking periods (from 1hour to 21 days) in SBF: (a) 2Si-5Ti, (b) 4Si-5Ti, (c) 2Si-20Ti, (d) 4Si-20Ti.**

After 21days of reaction the 4Si-5Ti and 2Si-5Ti present vibration bands due to P-O bending located around 460-610 $cm^{-1}$[39]. They are ascribed to the apatite formation, data which is in accordance with the SEM and XRD analyses. The intense band centred at 1080 $cm^{-1}$ was assigned to asymmetric stretching vibration of Si-O-Si bonds in amorphous silica [42]. Moreover, the FTIR spectra also shows an increase of the $OH^-$ groups

intensity after 24 hours for all studied samples, being a direct result of the substitution of the silanol groups with phosphate ones due to a charge balance. As for the 2Si-5Ti and 4Si-5Ti samples after 21 days incubation in SBF (Figure 23 (a)-(b)), an increase in the intensity of $PO_4^{3-}$ bands, located at ~465 $cm^{-1}$, was observed consecutively with the increase of the absorption bands from 572-650 $cm^{-1}$ and was attributed to the $OH^-$ groups from HAP [46].

Furthermore, the presence of apatite-like nanocrystalline phase for the 2Si and 4Si samples confirmed by XRD analysis is in good agreement with the SEM images (Figure 24 (A)-(B)). From these images one can observe that after 21 days of SBF immersion the crystals present a preferential orientation. The 4Si sample presents a small modification after 21 days of incubation, result which is in accordance with the XRD and FTIR analyses.

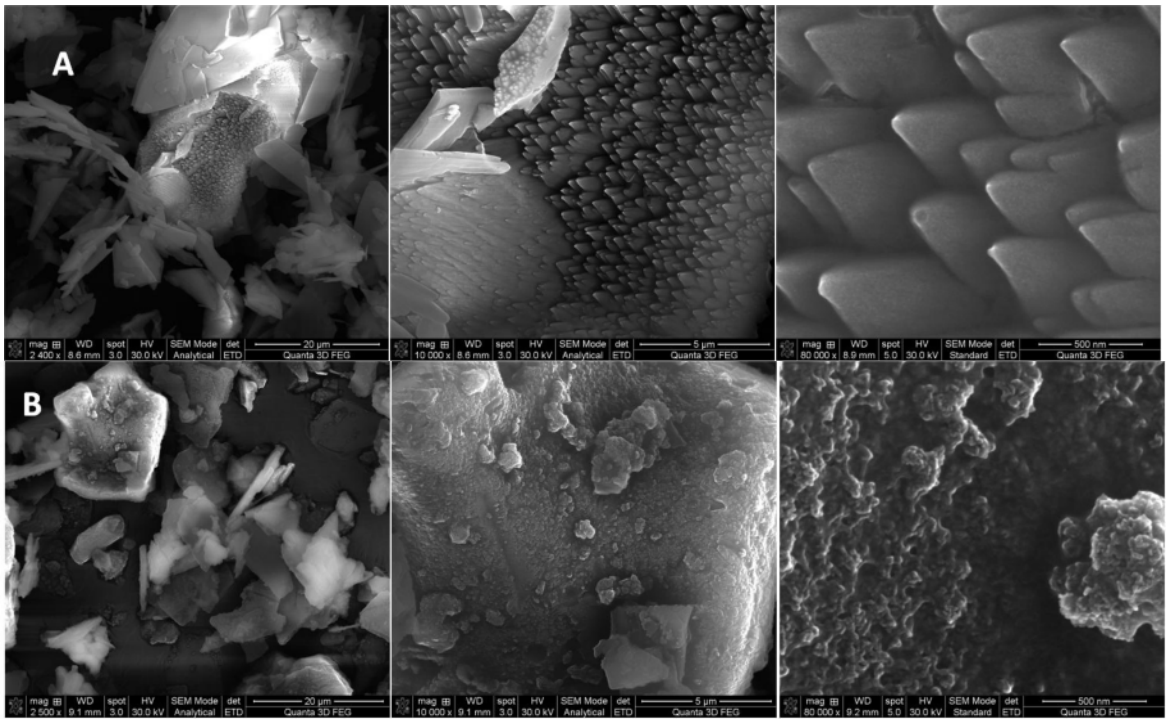


**Figure 24. SEM images of the surface of the materials after 21 days SBF incubation: (A) 2Si; (B) 4Si.**

Another important feature of the sol-gel materials is that after 21 days of immersion in SBF, the surfaces of the 2Si-5Ti and 4Si-5Ti glasses (Figure 25 (A)-(D)) reveal changes in their morphology developing structures of rod morphologies. Small modifications were observed for the samples with 20% $TiO_2$ after immersion (Figure 25 (B)-(D)) reflecting the high resistance to ionic exchange of the surface. Based on XRD data and SEM images, it could be concluded that new phases corresponding to HAP were formed on the materials surfaces with lower $TiO_2$ content.

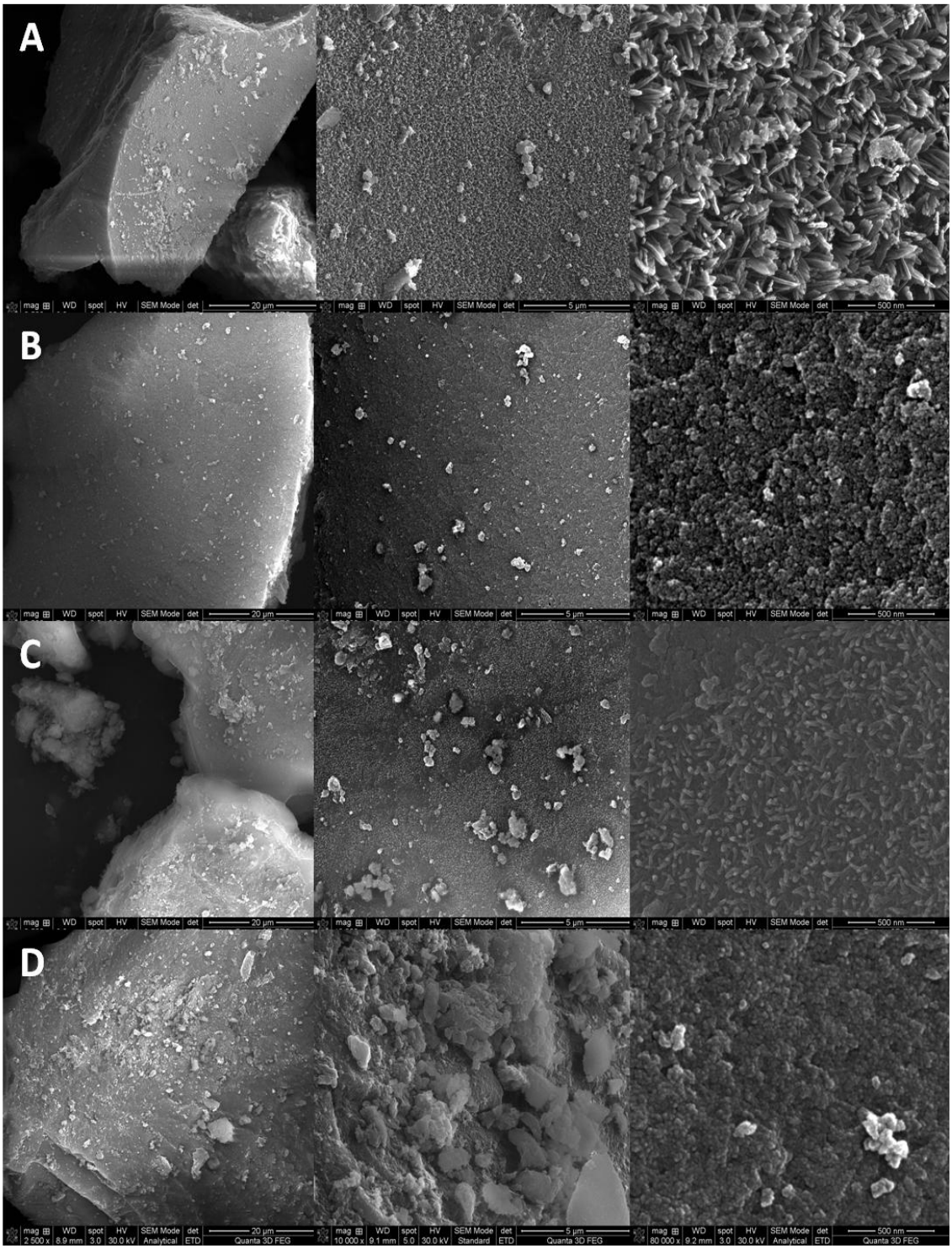


**Figure 25. SEM images of the glass samples after 21 days of immersion in SBF:**
**(A) 2Si-5Ti, (B) 2Si-20Ti, (C) 4Si-5Ti, (D) 4Si-20Ti.**

# 4. SELECTED CONCLUSIONS

Porous nanostructured materials belonging to the ternary $SiO_2CaO$-$P_2O_5$ and quaternary $SiO_2CaO$-$P_2O_5$-$TiO_2$ systems have been successfully synthesized by sol-gel method. It was shown by means of rheological and compression tests that one can predict the differences of mechanical properties between the studied samples.

It has been stated that the different gelation times, as well as the physical and morphological properties of the studied materials were governed significantly by the concentration of tetraethyl ester precursor and that of the solvent. Thus, $t_g$ was significantly speeded up and the elastic modulus was enhanced with the increase of the silica precursor amount. In addition, the elastic modulus was also enhanced by the increase of the titanium precursor concentration.

The thermal analysis of silica-calcium-phosphate and silica-calcium-phosphate with titanium dioxide samples, prepared by sol-gel method revealed endothermic events associated to dehydration and to decomposition processes.

It has been shown that the different thermal processing temperatures (350, 550 and 700°C) induce different separation of crystalline phases that dependent also by the silica content. The *in vitro* reactivity of these glasses can be predicted as function of their chemical composition (different precursor ratio, different solvent ratio); therefore the compositions of the glass samples were tested using various investigation techniques.

Based on the structural studies made on silica-calcium-phosphate glasses containing different amounts of $TiO_2$, it is concluded that CaO behaves as a network modifier for 5 mol% $TiO_2$. The addition of $TiO_2$ to the ternary silicate glass creates stronger Ti-O-P cross-linking within the glass network, which makes the glass denser and more resistant to degradation.

The main findings of this thesis are that, the lower silica (2Si) content exhibits bioactive behaviour compared with the highest one (4Si). Moreover, depending on the titania content (5 mol% $TiO_2$) and independent of the silica precursor content, one can obtain nanostructured materials with high specific surface area, bimodal pore size distribution showing bioactivity behaviour, when they are submerged in Kokubo's simulated body fluid up to 21 days. Further addition of $TiO_2$ (up to 20 mol%) leads to surface reconstruction when incubated into simulated body fluid. Thus, the silica-calcium-phosphate and the combination of these glasses with titanium dioxide are promising composites that could be exploited in several applications such as: tissue engineering, antimicrobial and environmental fields.

# SELECTED REFERENCES

[1]. Siqueira R.L., Peitl O., Zanotto E.D., Mater. Sci. Eng. C, 31, 2011, 983-991.

[2]. Rajesh P., Muraleedharan C.V., Komath M., Varma H., J. Mater. Sci.-Mater. M., 22(3), 2011, 497-505.

[3]. Roy M., Bandyopadhyay A., Bose S., Surf. Coat. Tech., 205 (8–9), 2011, 2785-2792.

[4]. Zhua Y., Wanga W., Jiaa X., Akasakab T., Liaoc S., Watari F., Appl. Surf. Sci., 2012, In Press.

[5]. Zan L., Fa W., Peng T., Gong Z.K., J. Photoch. Photobio. B, 86(2), 2007, 165-169.

[6]. Nath S., Tripathi R., Basu B., Mater. Sci. Eng. C, 29(1), 2009, 97–107.

[7]. Jiang P., Lin H., Xing R., Jiang J., Qu F., J. Sol-Gel Sci. Techn., 61(2), 2012, 421-428.

[8]. Oakenfull D.G., Parker N.S., Tanner R.I., "A method for determining the absolute shear modulus of a gel from a compression test", in "Gums and stabilisers for the food industry", vol.4, Eds. Phillips G.O., Williams P.A. & Wedlock D.J., Ed. IRL Press, Washington, U.S.A., 1988, p. 231-239.

[9]. Brunauer S., Emmett P.H., Teller E., J. Am. Chem. Soc., 60, 1938, 309 - 319.

[10]. Webb P.A., Orr C., "Analytical Methods in Fine Particle Technology", Ed. Micromeritics Instrument Corporation, Norcross, 1997, p. 81

[11]. Sing K.S.W., Everett D.H., Haul R.H.W., Moscou L., Pierrotti R.A., Rouquerlot J., Siemieniewska T., Pure Appl. Chem., 57(4), 1985, 603-619.

[12]. Kokubo T., Kushitani H., Sakka S., Kitsugi T., Yamamuro T., J. Biomed. Mater. Res., 24, 1990, 721-734.

[13]. Lacan P., Guizard C., Cot L., J. Sol-Gel Sci. Techn., 4(2), 1995, 151-162.

[14]. Datta S.S., Gerrard D.D., Rhodes T.S., Mason T.G., Weitz D.A., Phys. Rev. E, 84 (4-1), 2011, 041404-1-041404-6.

[15]. Jokinen M., Rahiala H., Rosenholm J.B., Peltola T., Kangasniemi I., J. Sol-Gel Sci. Techn., 12, 1998, 159-167.

[16]. Mason T.G., Bibette J., Weitz D.A., Phys. Rev. Lett., 75, 1995, 2051-2054.

[17]. Gaboriaud F., Nonat A., Chaumont D., Craievich A., J. Colloid Interf. Sci., 253, 2002, 140-149.

[18]. Simonsen M.E., Søgaard E.G., J. Sol-Gel Sci. Techn., 53, 2010, 485–497.

[19]. Nieto P., Dron R., Thevenot R., Zanni H., Brivot F., C.R. Acad. Sci. II B, 320(9), 1995, 485-488.

[20]. Bell N.S., Frischknecht A.L., Piech M., J. Disper. Sci. Technol., 32(1), 2010, 128-140.

[21]. Patnaik P., "Handbook of Inorganic Chemicals", (Eds.) McGraw - Hill Professional, 2003, p. 385-386.

[22]. Duff E.J., J. Appl. Chem. Biotechnol., 21(8), 1971, 233-235.

[23]. Singh G., Kapoor I.P.S., Mannan S.M., Kaur J., J. Hazard. Mater. A, 79, 2000, 1-18.

[24]. Safronova T.V., Kuznetsov A.V., Korneychuk S.A., Putlyaev V.I., Shekhirev M.A., Cent. Eur. J. Chem., 7(2), 2009, 184-191.

[25]. Madhurambal G., Subha R., Mojumdar S.C., J. Therm. Anal. Calorim., 96(1), 2009, 73-76.

[26]. Frost R.L., Palmer S. J., Thermochim. Acta, 521, 2011, 14-17.

[27]. Ragai J., J. Chem. Techol. Biot., 40, 1987, 75-83.

[28]. Acik O., Madarász J., Krunks M., Tonsuaad K., Pokol G., Niinistö L., J. Therm. Anal. Calorim., 97(1), 2009, 39-45.

[29]. Nakayama N., Hayashi T., Colloid Surf. A-Physicochem. Eng. Asp., 317, 2008, 543-550.

[30] **Taloş F.,** Vulpoi A., Simon S., Studia Chemia (2012) (accepted).

[31] **Taloş F.,** A. Ponton, S. Simon, Viscoelastic and spectroscopic investigation of silica calcium-phosphate sol-gel biomaterials, submitted paper.

[32]. **Taloş F**., Ponton A., Simon S., Proceedings of « Le 46$^{-eme}$ Congrès Annuel du Groupe Français de Rhéologie (GFR) », 2011, 4 pp.

[33] Saravanapavan P., Hench L.L., J. Non-Cryst. Solids, 318(1-2), 2003, 1-13.

[34]. Socrates G., "Infrared and Raman characteristic group frequencies: tables and charts", Ed. John Wiley and Sons, 2004.

[35]. Boccaccini AR, Erol M, Stark WJ, Mohn D, Hong Z, Mano JF, Compos Sci Technol 70(13), 2010, 1764–1776.

[36]. Sing K.S.W., Everett D.H., Haul R.H.W., Moscou L., Pierrotti R.A., Rouquerlot J., Siemieniewska T., Pure Appl. Chem., 57(4), 1985, 603-619.

[37]. Shaim A., Tabirou M-Et, Montagne L., Palavit G., Mater. Res. Bull., 37(15), 2002, 2459-2466.

[38]. Mamaeva V., Sahlgrena C., Lindén M., Adv. Drug Deliver. Rev., 2012, In Press.

[39]. Melinte G., Baia L., Simon V., Simon S., J. Mater. Sci., 46, 2011,7393-7400.

[40]. Belkhouaja M., Tabirou M. Et., Elmoudane M., Phase Transit, 76, 2003, 645-652.

[41]. Vulpoi A., Baia L., Simon S., Simon V., Mater. Sci. Eng. C, 32, 2012, 178–183.

[42]. Filho O.P., LaTorre G.P., Hench L.L., J. Biomed. Mater Res., 30, 1996, 509-514.

[43]. Wang C.C., Ying J.Y., Chem. Mater., 11(11), 1999, 311 –3120.

[44]. Svetlakov N.V., Nikitin V.G., Nikolaeva E.A., Russ. J. Org. Chem., 43(5), 2007, 771-772.

[45]. Pereira M. M., Clark A.E., Hench L.L., J. Am. Ceram. Soc., 78(9), 1995, 2463-2468.

[46]. Chrissanthopoulos A, Bouropoulos N., Yannopoulos S.N., Vibrat. Spec., 48, 2008, 118-125.

# Acknowledgments

I express my deepest gratitude to my supervisor **Prof. Dr. Simion Simon** for offering me excellent guidance, support and great patience during my doctoral research period.

With the utmost gratitude, I would like to thank **Prof. Dr. Viorica Simon** for the useful discussions and good advices.

I would like to extend my gratitude to my research internship supervisor, **Prof. Alain Ponton** from **Matter & Complex Systems Laboratory** of *"Paris Diderot University, Sorbonne Paris Cité"*, France, for his invaluable guidance, constructive instructions and for the wonderful opportunity to achieve additional knowledge in the rheological field.

I would like to thank **Assoc. Prof. Lucian Baia** and **Assoc. Prof. Raluca Ciceo Lucăcel** for the scientific discussions, good advices during my doctoral research period.

My sincere gratitude and thanks goes to my committee members for proofreading of the thesis: **Prof. Dr. Felicia Iacomi** from *A. I. Cuza University, Iasi*, **Prof. Dr. Eugen Culea** from *Technical University of Cluj-Napoca*, **Prof. Dr. Mihai Todica** from *Babeş-Bolyai University*.

I wish to express many thanks to my dear colleagues from Faculty of Physics and from Institute of Interdisciplinary Research on Bio-Nano-Sciences for their help and scientific advices: dr. A. Vulpoi, dr. O. Ponta, dr. C. Gruian, dr. D. Trandafir, R. Vereş, dr. E. Vanea, dr. M. Mureşan Pop, dr. M. Tămăşan, dr. K. Magyari, dr. T. Radu. My thanks go to my colleagues from MSC Laboratory who has been great support and encouragement during my internship in Paris.

My most heartfelt thanks go to my family for always encouraging and supporting me. Especially to my dear sister Nicoleta, to my aunts: Marioara and Doina. Last, but certainly not the least, I wish to thank for the permanent support to Ardelean and Tolgyi families.

Finally, I would like to thank POSDRU/88/1.5/S/60185 for financial support during this PhD.

Florentina Taloş

Cluj-Napoca, December 2012